Squaramide-based interpenetrated networks for load-bearing applications

Chen, Y.

Chapter 5

Photothermal Filamentous Supramolecular and Covalent Double Network Hydrogels

Hybrid supramolecular and covalent double network hydrogels have drawn great attention due to their stiff and tough mechanical characters that can approximate the structure and function of load-bearing tissues. The use of nanoparticles in these networks provides opportunities to augment their mechanics and introduce responsive behaviors that can be remotely triggered with stimuli such as light for their eventual application as therapeutic materials. Herein, we introduce 15 nm gold nanoparticles with 1,2-dithiolane end-functionalized capping groups into the hydrogels that can be simultaneously crosslinked with the covalent and supramolecular networks containing the same reactive group and norbornene through photopolymerization. The addition of gold nanoparticles enhanced the double network hydrogel's mechanical characteristics, especially their energy dissipation property, and conferred tunable conductivity and photothermal properties consistent with the Au@PEG-DT concentration. The double network hydrogels showed injectability prior to photopolymerization and stayed stable in PBS after crosslinking. Stimulation of the plasmonic-photothermal effect of the gold nanoparticles with a laser light source at 532 nm enabled ablation of MDA-MB-231-B1 cells at precise positions in 3D cell culture.

This chapter was prepared as a research article: Ying Chen, Marijn van den Brink, Thomas J.F. Kock, Roxanne E. Kieltyka*

5.1 Introduction

Hydrogels are three-dimensional (3D) materials composed of crosslinked polymer chains to form a network that able to retain a high content of water and have found many applications in the fields such as tissue engineering, drug delivery, soft robotics, and others.[1-5] They have been extensively used as synthetic platforms to closely mimic native tissues due to their tunable physical properties, structural similarity and easy modification with biological cues.[6-8] However, hydrogels are usually applied as single networks that are brittle, limiting their ability to mimic the mechanically loaded stiff tissues.[9,10] To overcome this challenge, double network (**DN**) hydrogels can be formed, where a second polymer network is added to create a structure that exhibits higher mechanical strength and enhances energy dissipation when compared to traditional single hydrogel networks.[11-18] When filamentous supramolecular polymers are used as a sacrificial network they can impart these materials with features that mimic the structures and functions of biopolymers of the extracellular matrix (ECM).[19-23] These mechanical behaviour of these networks that arise due to the non-covalent character of the assemblies can further increase the recovery of the hydrogels, opening up new avenues to prepare hydrogels that mimic ECM properties for 3D cell culture in a wide range of applications.[19,23-25] The often-used chemical strategies only permit mechanical tuning of the materials, however their combination with stimuli-reponsive components can open the door to a wider range of biomedical applications including those that are therapeutic.[26-28]

The incorporation of nanoparticles (e.g., gold nanoparticles, graphene) is another strategy used to augment hydrogel mechanical properties.[29-34] Nanoparticles are embedded in the pores of the network through chemical and/or physical interactions with the network,[34-36] resulting in increased stiffness (0.01-1000 times) and toughness (0.01 - 1 MJ/m^{-3}), as well as improved energy dissipation capabilities.[29-32] This enhancement of mechanical properties is contingent upon the hybrid network's capacity to alleviate stress concentration through dynamic exchanges between polymer segments anchored to the particles and unabsorbed polymer strands.[37-40] Additionally, the nanoparticles can bring additional functions[41-47] consistent with their composition such as heat generation, electrical conductivity[48,49] and magnetic properties that can be attractive for diverse range of biological applications. In particular, gold nanoparticles due to their adaptable modification, and extraordinary optical and plasmonic properties[50,51] have been examined for their capacity to alter hydrogel mechanics while providing access to conductivity and the photo-thermal effect that is attractive for cancer therapy.[26,27] However, in many gold nanoparticle-integrated hydrogels, the particles are physically suspended instead of being crosslinked to the hydrogel network causing aggregation that leads to heterogeneity of material properties. Furthermore, most research efforts have been directed towards enhancing the mechanical properties of hydrogels based on natural polymers using gold particles, while there are few examples of synthetic hydrogels in this area.

We previously developed a **DN** hydrogel that shows biomimetic mechanical properties that are cartilage-like by crosslinking of a supramolecular and covalent polymer network through poly(disulfide) and poly(disulfide-norbornene)s. The **DN** consists of squaramide-based monomers[52]and covalent poly(ethylene glycol) polymers[53] that could sustain 14 days of cyclic compressive loading in 3D cell

culture. (**chapter 3**). Because gold nanoparticles can further impact the mechanical properties of the network while introducing a handle for stimuli-responsiveness due to the photothermal effect of the particles, we became interested in understanding their impact on the hybrid **DN** presented in Chapter **3**. To improve the dispersion and stability of AuNPs in **DN** hydrogels, the nanoparticles were functionalized with heterobifunctional oligo(ethylene glycol polymers) containing a thiol unit that can bind strongly to the gold surface and a 1,2-dithiolane for coupling to the **DN** simultaneously during its crosslinking with UV light at 365 nm. We then analyze the injectability, mechanics, conductivity, and photo-thermal effect of these networks, gaining insight into their potential to tune the behavior of this double network gel based on the nanoparticle concentration used. Finally, we demonstrate the acquired photo-thermal properties of the **DN** hydrogel with gold nanoparticle addition by the selective ablation of bone tumor cells with spatial control.

5.2 Results and Discussion

Nanocomposite double network hydrogel design and synthesis

A 4-arm poly(ethylene glycol) (PEG) macromonomer (in total 3 wt%) end-functionalized with DT or NB (PEG_4-DT or PEG_4-NB) composes the first network of the **DN** and **DN-Au** hydrogels (Scheme 1). These macromonomers were synthesized in one-step using carbodiimide coupling chemistry yielding a high degree of functionalization similar to the earlier reported linear macromonomers.[53] UV irradiation with lithium phenyl-2,4,6-trimethylbenzoylphosphinate (LAP, 1mM) lead to crosslinking of these two monomers to form a single network hydrogel material. The second network is a multicomponent supramolecular polymer consisting of tripodal squaramide-based monomers, including one outfitted with DT that is added in a 10 mol% (**SN**, 4 mM) ratio.[52] To prepare the **DN** hydrogels, we combine the DT and NB macromonomers into the supramolecular filaments in phosphate-buffered saline (pH 7.4) after sonication on ice. We then allowed the solution to reach room temperature (RT), to form the polymer hydrogel.

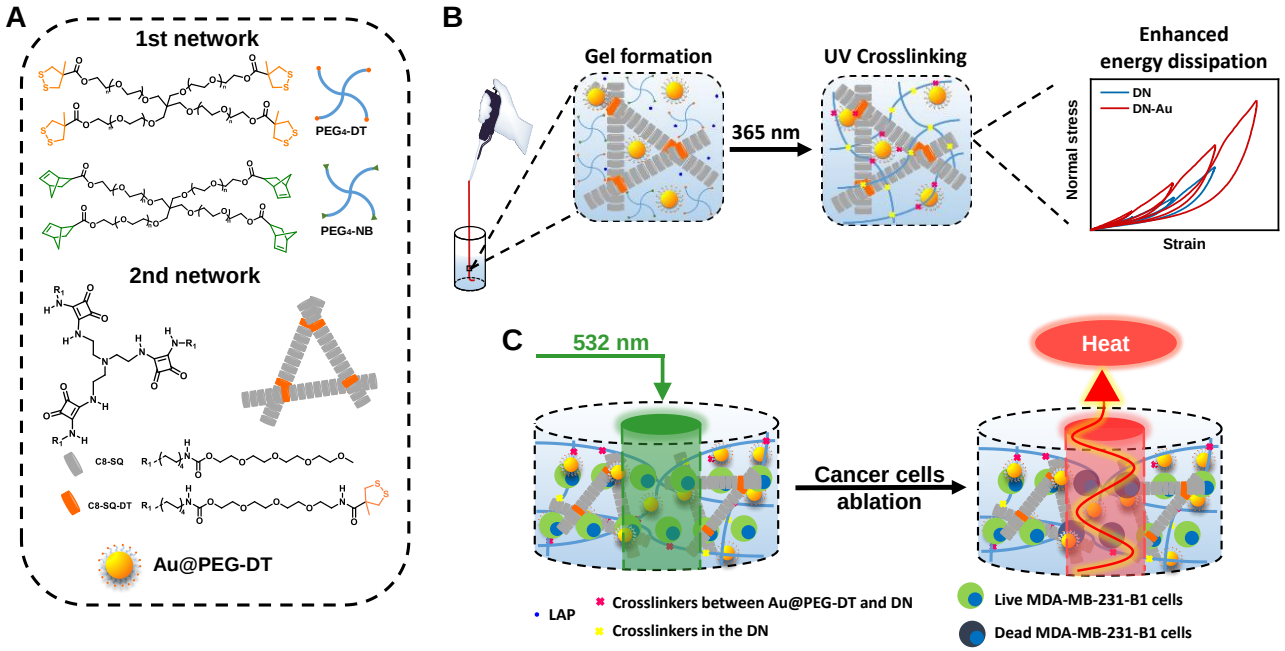

Scheme 1. (A) Double network hydrogels and components used in this study. (B) Extruded **DN-Au** hydrogel and subsequent **DN** photopolymerization strategy. (C) Photo-thermal effect of crosslinked gold nanoparticles (AuNPs) in the 3D **DN** hydrogel MDA-MB-231-B1 cells with light irradiation.

Next, we used the citric acid reduction process[54,55] to prepare citrate-coated gold nanoparticles (15 nm, Au@Citrate) and coupled them with SH-PEG_{5400}-DT (Mw: 5.4 kDa) to form a PEG shell around the particle with reactive groups (DT) for coupling to the **DN** (Figure S1).[53] Here, we synthesized SH-PEG_{5400}-DT by reacting linear thiol-PEG-hydroxy and DT with carbodiimide coupling chemistry resulting in a high degree of end-functionalization.[53] Relying on the stronger chemisorption of thiols on the gold surface relative to DT[56,57], we expected that the 1,2-ditholane units reside on the periphery of the PEG shell and available for crosslinking with the dithiolane network. We confirmed this by ^{1}H-NMR spectroscopy comparing the -CH_2 and -CH_3 protons on DT (3.05-2.9 ppm, 1.48-1.35 ppm) from the SH-

PEG_{5400}-DT coated gold nanoparticles (Au@PEG-DT) to that on SH-PEG_{5400}-DT polymer, where no discernable changes in chemical shift was found (Figure S2). The Au@PEG-DT nanoparticles retained their structure after the exchange of the capping group for the PEG with the DT unit, as demonstrated by red-shifting of the band at 518nm of Au@Citrate to 522nm with the addition of SH-PEG_{5400}-DT (Figure 1A). The transmission electron microscopy (TEM) and dynamic light scattering (DLS) further supported these results (Figure 1B-C, S3), pointing out that introduction of the DT at the periphery of the capping group does not have an impact on particle size or cause aggregation. Moreover, replacement of the PEG capping group lead to the effective exchange of citrate as evidenced by the significant change in zeta potential of the gold nanoparticles (AuNPs), from ~ -40.30 mV to ~ -21.26 mV for Au@Citrate and Au@PEG-DT, respectively (Figure 1D). As a control, we also synthesized Au@PEG nanoparticles lacking the DT group that showed similar optical and morphological properties to the Au@PEG-DT.

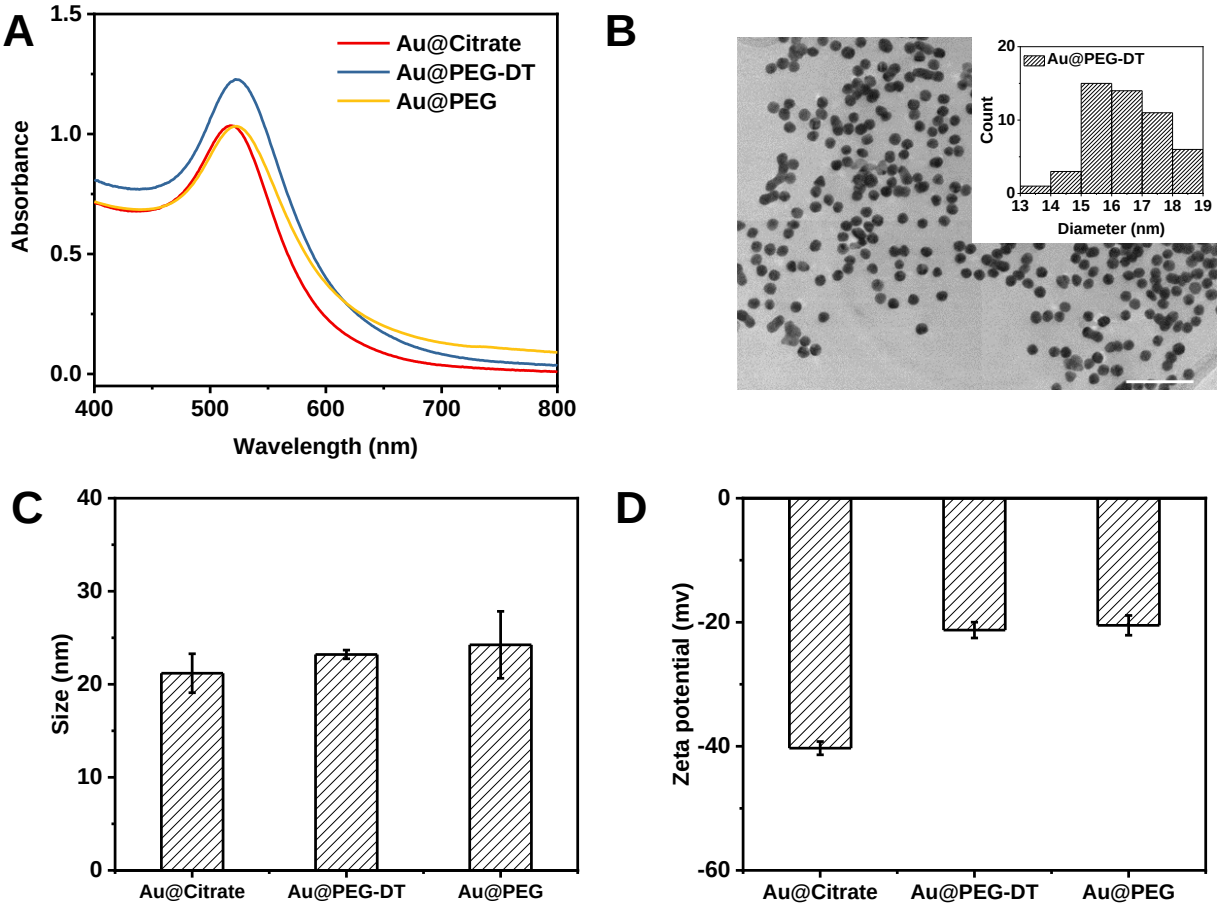

Figure 1. Characterization of AuNPs in water. (A) UV spectra of Au@Citrate and Au@PEG-DT. (B) TEM image of Au@PEG-DT (300 µg/ml). Scale bar: *100 nm*. (C) Hydrodynamic diameters of Au@Citrate and Au@PEG-DT measured by DLS. (D) Zeta potential of Au@Citrate and Au@PEG-DT. Mean ± SD, N ≥ 3.

We then prepared double network hydrogels **DN-Au$_x$** crosslinked with Au@PEG-DT particles under UV light at ~365 nm and a photoinitiator lithium phenyl-2,4,6-trimethylbenzoylphosphinate (LAP, 1mM). To permit efficient crosslinking of the hydrogels and subsequent imaging of 3D cell cultures, we kept the Au@PEG-DT at 1 mg/mL for the remainder of the study to high light transmittance. The crosslinking of these particles to the supramolecular and covalent polymer networks components yielded NB-DT and DT-DT bonds depending the ratio of the various components.[53] We then explored the impact of gold nanoparticles on the formation of the double network gels. The resulting **DN-Au** hydrogels appeared wine red in color varying in intensity from light to dark red depending on Au@PEG-DT concentration, even after photopolymerization as observed in gel inversion tests (Figure S4).

Quantification of mechanical properties of DN and DN-Au hydrogels

We probed the effect of adding Au@PEG-DT to the filamentous double network hydrogel on its mechanical properties using oscillatory rheology. In time sweep measurements, the storage modulus (G') of the **DN** network increased from ~80 Pa before UV exposure to ~10.12 kPa after crosslinking (Figure 2A and S5), and was comparable with the results for the **DN** in **Chapter 3**. When Au@PEG-DT increased from 0.1 mg/mL (**DN-Au$_{0.1}$**) to 0.25 mg/mL (**DN-Au$_{0.25}$**), the stiffness of crosslinked hydrogels increased from ~11.32 kPa to ~13.04 kPa, while further raising the nanoparticle concentration up to 1.0 mg/mL (**DN-Au$_{0.5}$** and **DN-Au$_{1.0}$**) led to slower rate of stiffness increase and steady decrease of the storage modulus (from ~10.22 kPa to ~7.34 kPa, respectively). This decrease in storage modulus is likely due to the reduced transmission of UV light through the uncrosslinked **DN-Au** gels due to the increased nanoparticle concentration that can interfere with the photopolymerization process. We exchanged Au@PEG-DT for 0.25 mg/mL Au@PEG that lacks the DT moiety to compare the effect of covalent crosslinking of the gold nanoparticles on the **DN** gel. The storage modulus of the **DN-Au@PEG$_{0.25}$** hydrogel with the same UV exposure as the **DN-Au$_{0.25}$** hydrogel showed slower rise in the storage modulus reaching a lower value than the **DN-Au$_{0.25}$** gel crosslinked with Au@PEG-DT of ~10.82 kPa (Figure S6A). The frequency sweep showed that this hydrogel is independent of the frequency from 0.1 Hz to 10 Hz (Figure S7). Strain sweeps claimed that the hydrogels were stable at low strain (<100%) and could break when the strain was higher than 200 %. Step-strain test sweep demonstrated that the uncrosslinked **DN-Au$_{0.25}$** hydrogel has excellent self-healing property (Figure S8). These results suggest that the gold nanoparticles are chemically crosslinked to the **DN** hydrogel and contribute to its mechanical properties as a function of their concentration.

Because of the capacity of nanocomposites to enhance the mechanical characteristics of **DN** hydrogels in compression,[58-60] we further evaluated the behaviour of the **DN-Au** networks under this type of mechanical load. Axial force compression tests in the rheometer demonstrated that inclusion of Au@PEG-DT at 0.25 mg/mL in the **DN** network increased the fracture strain from ~18.34 % to ~20.27 % and the compression modulus rose from ~492.62 kPa to ~574.86 kPa (Figure 2B-E, Table 1). Additionally, the **DN** hydrogels showed improved toughness with the addition of the gold nanoparticles, rising from ~11.84 to ~14.68 J/m^3, on par with other nanocomposite enhanced hydrogels.[61,62] Consistent with the decrease in stiffness when increasing the Au@PEG-DT concentration from 0.25 mg/mL to 1 mg/mL,

these hydrogels also showed a reduced ability to sustain compressive loads in contrast to the **DN** hydrogel without the added gold particles. At an Au@PEG-DT concentration of 1 mg/mL (**DN-Au$_1$**), the

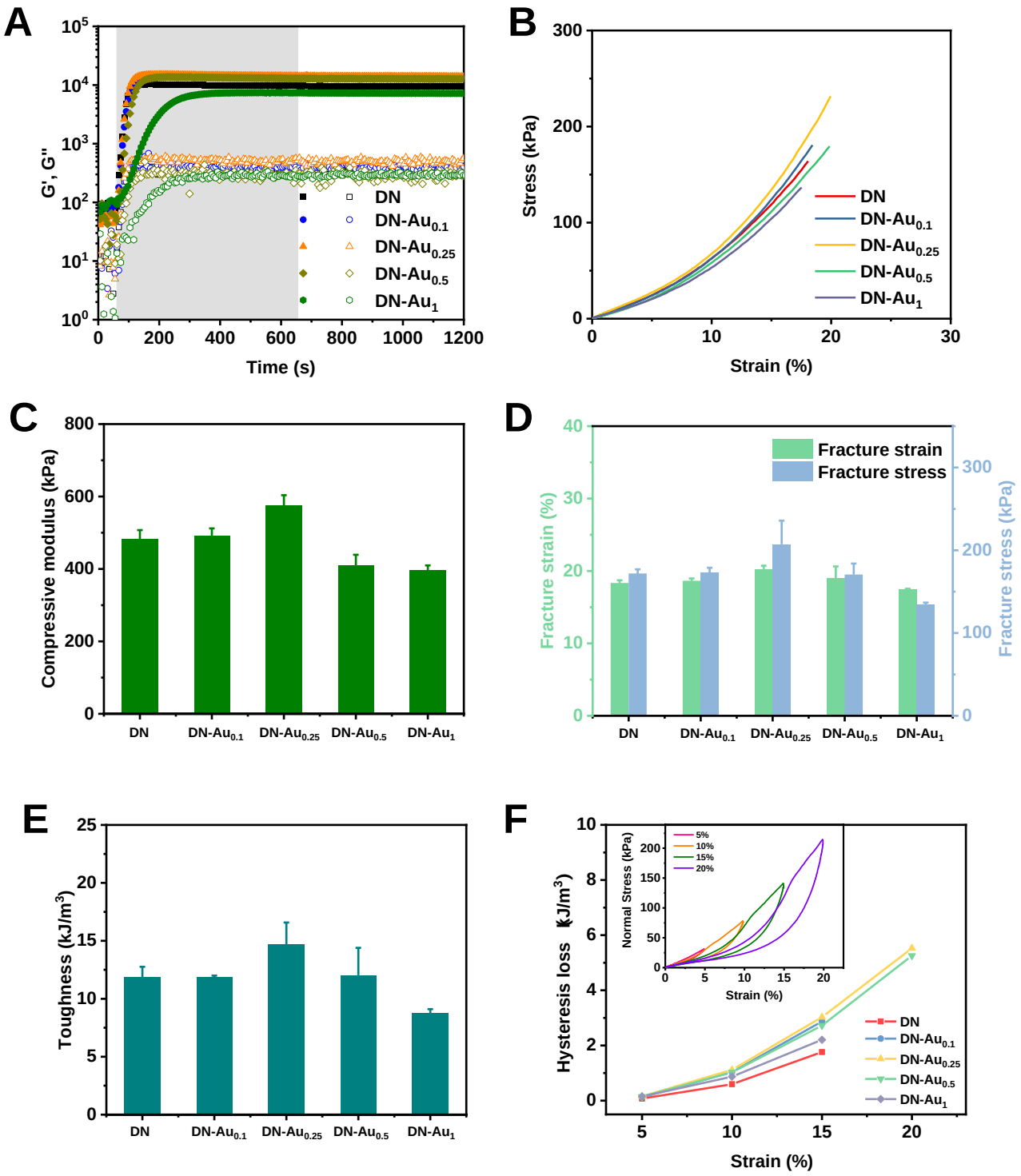

Figure 2. Mechanical properties of **DN** and **DN-Au** hydrogels measured at a constant compression speed (10 μm/s): (A) Oscillatory rheology time sweep measurements of hydrogels with varied Au@PEG-DT concentrations before and after 10 min UV irradiation using a fixed strain (γ = 0.05%) and frequency (ƒ = 1.0 Hz) at room temperature. Grey regions indicate UV exposure. (B) Uniaxial stress-strain curves. (C) Compressive modulus. (D) Compressive fracture strain and stress. (E) Compressive toughness. Mean ± SD, N ≥ 3. (F) Hysteresis loss of photocrosslinked **DN** and **DN-Au** hydrogels. Insert: Cyclic

hysteresis curves of photocrosslinked **DN-Au$_{0.25}$** hydrogel at different maximum strains (γ_{max}) using a loading-unloading test. Conditions for UV irradiation: ~10 mW/cm^2, 320-500 nm filter with maximum absorbance at 365 nm.

hydrogel showed a reduced fracture strain of ~17.50%, compressive modulus at ~396.81 kPa and toughness of ~8.77J/m^3. Addition of the Au@PEG nanoparticles **DN-Au@PEG$_{0.25}$** resulted in a higher fracture strain (~20.03%) but a reduced fracture stress (~154 kPa) and fracture energy (~8.75 kJ/m^3) in contrast to the **DN** hydrogel lacking nanoparticles (Figure S6B-6D). Hence, the nanoparticle crosslinkers can enhance the compressive mechanical properties of the supramolecular and covalent **DN** as the lack of chemical bonding reduces their response to compression.

We further examined the effect of the cross-linked AuNPs on the energy dissipation properties of **DN** and **DN-Au** hydrogels by compressive loading-unloading cycles at different maximum compression strains (λ_{max}) increasing from 5 to 25 %. All **DN-Au** exhibited obvious hysteresis loops that increased in parallel with the compression strain (λ_{max}) like the DN hydrogel (Figure 2F and S9). For example, the dissipated energy of **DN-Au$_{0.25}$** increased from ~0.16 kJ/m^3 (λ_{max} = 5%) to ~5.53 kJ/m^3 (λ_{max} = 25%). In contrast, the **DN** network in the lacking Au@PEG-DT showed a reduction in the dissipated energy from 0.12 (λ_{max} = 5%) to ~1.76 kJ/m^3 (λ_{max} = 15%) and the one with Au@PEG (0.25 mg/mL) that lacking DT for crosslinking falls in the range of ~0.11 to ~2.61 kJ/m^3 (λ_{max} = 15%) (Figure S10). These results indicate that physical introduction of the gold nanoparticles improve the energy dissipation properties of **DN-Au** hydrogels and their dynamic-covalent crosslinking through DT can further enhance this property.

Table 1. Fracture strain, facture stress, fracture energy and compression modulus of **DN** and **DN-Au** hydrogels under 10 µm/s speed, Mean ± SD, N ≥ 3.

Name	Fracture strain (%)	Fracture stress (kPa)	Fracture energy (kJ/m^3)	Compression modulus (kPa)
DN	18.34 ± 0.37	171.81 ± 5.06	11.84 ± 0.92	492.62 ± 27
DN-Au$_{0.1}$	18.6525 ± 0.61	172.81 ± 6.13	11.873 ± 0.12	491.41 ± 20.57
DN-Au$_{0.25}$	20.27 ± 0.46	207.45 ± 28.38	14.68 ± 1.90	574.86 ± 18
DN-Au$_{0.5}$	18.97 ± 1.65	170.66 + 13.30	12.03 ± 2.37	408 ± 30.49
DN-Au$_{1}$	17.50 ± 0.019	134.52 ± 2.81	8.77 ± 0.33	396.81 ± 19
DN-Au@PEG$_{0.25}$	20.07 ± 3.60	158.63 ± 20.6	10.94 ± 0.37	426.81 ± 25.43

Structural characteristics of the DN hydrogel

We performed electron microscopy and equilibrium swelling experiments to gain insight into the structural characteristics of the **DN-Au** hydrogels that underlie the recorded rheological changes with Au@PEG-DT addition. In (cryogenic) transmission electron microscopy (Cryo-TEM) the **DN** and **DN-Au** solutions showed long and flexible (~5 nm nm) filamentous structures even after crosslinking with well-dispersed Au@PEG-DT throughout the **DN-Au** hydrogels that lacked aggregation (Figure S11-S12).

Moreover, some AuNPs appeared associated with the supramolecular filaments, most likely due to photocrosslinking of the squaramide-based DT monomers with the Au@PEG-DT nanoparticles. We further probed the **DN** and **DN-Au** hydrogel structures at the microscale after UV exposure by scanning electron microscopy (SEM). The pore size of the **DN** hydrogel (~13 µm) decreased slightly with the incorporation of Au@PEG-DT at 0.5 mg/mL (~12 µm). Increasing the concentration up to 1 mg/mL resulted in an even smaller pore size (~8 µm) filled with nanoparticles and blurred pore edges (Figure S13). The micrometer scale of the pores likely arises due the freeze-drying method used to prepare the gels for imaging. These observations point to a difference in network structure with increasing gold nanoparticle concentration and align with the earlier measured reduced mechanics by oscillatory rheology. These studies demonstrate that the **DN** and **DN-Au** hydrogels exhibit a filamentous nature with sufficiently large pore sizes that can be tuned by nanoparticle concentration, rendering them suitable for 3D cell culture application.[63,64]

To gain insight into the extent of crosslinking and retention of Au@PEG-DT in the **DN** for their subsequent applications in 3D cell culture, we conducted an equilibrium water content and gel stability assays. We prepared the **DN** and **DN-Au** hydrogels above the CGC (critical gelling concentration)[65] and photocrosslinked them with 10 min UV irradiation (375 nm), (Figure 3) the photocrosslinked hydrogels on day 2 were 20-30 times heavier than the starting materials.[66] The decline in swelling ratio among the samples can be attributed to the increase in polymer and nanoparticle concentrations. Gel stability tests display that the **DN** and **DN-Au** hydrogels retained approximately 100% of their initial weight for 15 days without degradation in water. We then investigated the diffusion of AuNPs@PEG-DT using UV measurements and observed a minimal release of AuNPs from the network (Figure S4), further pointing out their effective covalent crosslinking to the materials. These results showed that the maintenance of the gels and gold nanoparticles within them after several media changes, showed that the materials can sustain conditions typically associated with 3D cell culture.

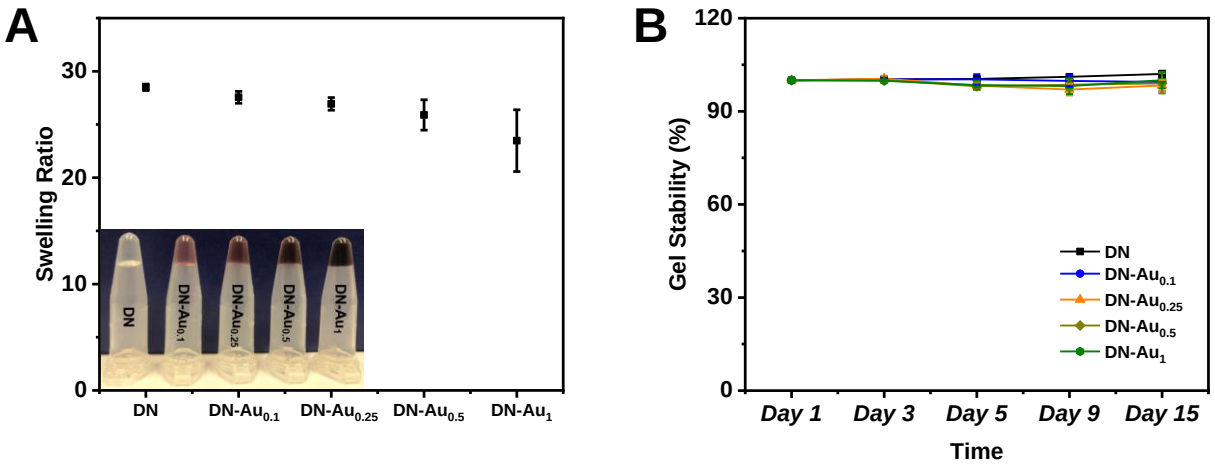

Figure 3. DN and **DN-Au** hydrogels (A) Swelling ratio. Insert: digital photo inverted hydrogels tested. (B) Gel stability tests over 15 days.

Evaluation of DN-Au hydrogel conductive and photothermal properties

AuNPs can confer additional features to hydrogel materials such as conductivity and photohermal behaviour due to their inherent physicochemical properties.[67-69] We performed a set of electrochemical performance tests to understand the relationship between the Au@PEG-DT concentration and the **DN-Au** hydrogel conductive properties. When Au@PEG-DT concentration increased from 0 mg/mL to 1 mg/mL, the conductivity rose modestly from ~8.22 x 10^{-4} S/m to ~9.88 x 10^{-4} S/m (Figure 4A). These findings are in line with other metal nanoparticle-hydrogel networks that report similar subtle increase in conductivity.[70]

Besides their conductivity, the optical absorption characteristics of AuNPs allow for conversion of incident light into thermal energy.[71] We tested the photo-thermal effect of the **DN** and **DN-Au** hydrogels using a 1 W 532 nm visible light source and a sensitive thermometer. Hydrogels with a higher Au@PEG-DT concentration resulted in a greater temperature increases when irradiated under the same condition (Figure 4B). Incorporation of Au@PEG-DT raised the gel temperature to ~71.05°C in **DN-Au$_{0.1}$**, and further increasing their concentration in **DN-Au$_{0.5}$** drove a temperature increase of relative to **DN**. On removing the light source, the **DN** and **DN-Au** hydrogels cooled down to room temperature after 10 minutes. This photo-thermal effect could be cycled at least 3 times without attenuation. We then assessed extrudability of the uncrosslinked **DN-Au** hydrogels for their eventual application as inks for printing applications or as injectable materials. The **DN-Au$_{0.25}$** hydrogel can be extruded into a noodle shape using a micropipette (Figure 4C-D). We then applied the crosslinking process to the extruded gel with a benchtop LED at 375 nm for 10 min. The photopolymerized material retains its shape in water, showing potential for 3D printing applications.

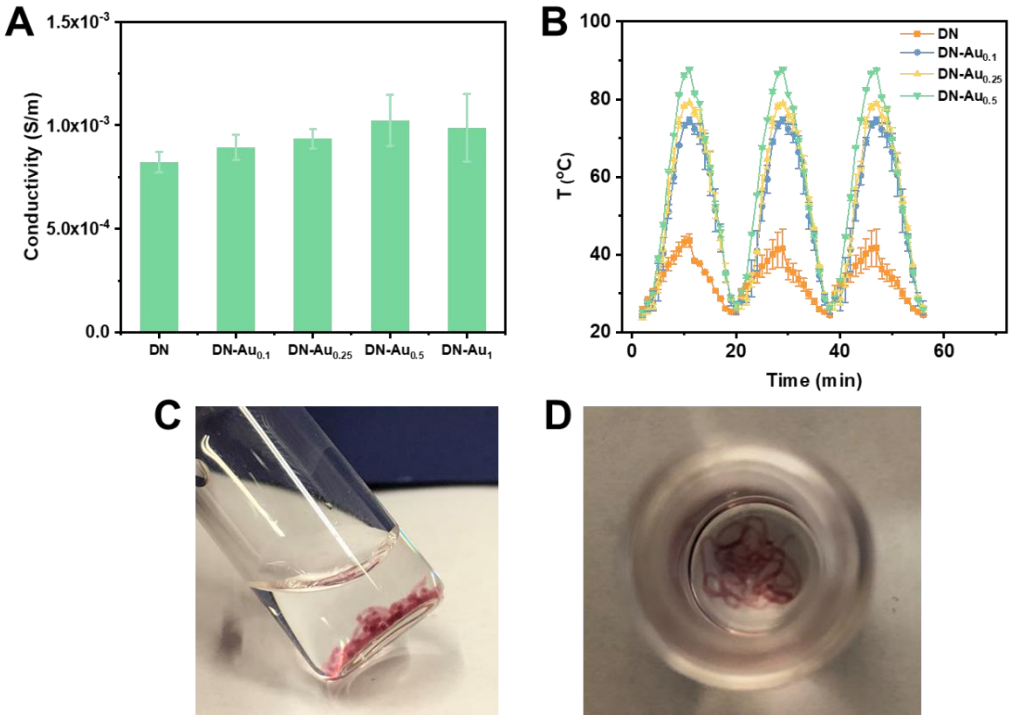

Figure 4. (A) Conductivity of different crosslinked **DN** and **DN-Au** hydrogels. (B) Cyclic photo-thermal effect of crosslinked **DN** and **DN-Au$_{0.1}$** - **DN-Au$_{0.5}$** hydrogels irradiated with light at 532 nm. Digital photos of extruded **DN-Au$_{0.25}$** after photopolymerization and kept in water for 1 day: (C) side view. (D) top view.

Photothermal ablation of cancer cells in DN-Au hydrogels

The photothermal property of AuNPs is attractive for cancer therapy applications *in vivo* where the focus is on tumor cell ablation in a highly selective and minimally invasive manner.[72-78] To examine the suitability of composite **DN-Au** hydrogels for cell ablation, we first assessed cell viability of encapsulated NIH 3T3 fibroblasts in the various hydrogel compositions and concentrations. We observed high cell viabilities reaching over 90% after 24h culture and 80% after 48h in 3D culture with 5 min 375 nm UV exposure (Figure S14-S15) by a Live/Dead Assay with calcein AM/propidium iodide staining.

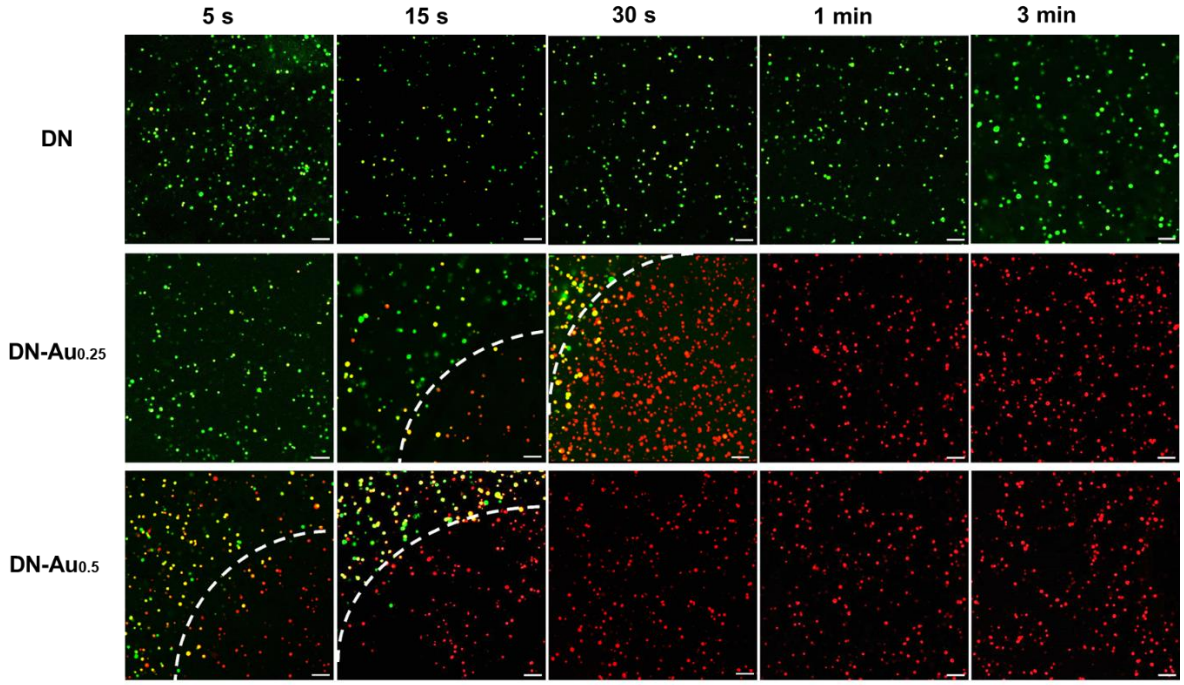

Figure 5. Confocal microscopy images of stained live (calcein AM) and dead (propidium iodide) MDA-MB-231-B1 cells encapsulated and incubated in **DN** and **DN-Au** in 3D for 24 h and subsequently irradiated under a 532 nm (1 W) visible light laser for varying time intervals. Scale bar: *100 µm*.

Next, we explored the capacity to selectively ablate a cancer cell line from bone metastases, MDA-MB-231-B1, within **DN-Au** hydrogels using green light. Cell viability of MDA-MB-231-B1 cells in crosslinked **DN** and **DN-Au** hydrogels after 24 h culture in the absence of green light was over 90% (Figure S16-S17). We then assessed the photothermal effects of the **DN** and **DN-Au** hydrogels on cell viability by a Live/Dead stain after irradiating the cancer cell-laden hydrogels in 3D with a 532 nm visible light laser (1 W) at different time points (0 s - 3 min). Application of the light source on the **DN** hydrogel without gold nanoparticles could not cause cell death even with a 3 min exposure (Figure 5 and S18). In contrast, the **DN-Au$_{0.5}$** could efficiently convert the light into heat and induce cell death within 5 s,

while the **DN-Au$_{0.25}$** hydrogel needed a longer exposure time of 15 s to observe the same effect. These results align with earlier photothermal data where greater Au@PEG-DT concentrations resulted in a larger temperature increase in the hydrogels. Furthermore, upon brief irradiation of the **DN-Au** hydrogels, we found that the dead cell area expanded proportionally with both the concentration of Au@PEG-DT and the duration of irradiation, resulting in non-viable cells across the **DN-Au$_{0.25}$** and **DN-Au$_{0.5}$** hydrogels after a 3-minute light exposure. These results indicated that the photoablation position can be precisely controlled by the 532 nm laser or the gold nanoparticle concentration. These findings demonstrate a positive correlation between the concentration of AuNPs and light dosage on cell photoablation, and the irradiated position can be precisely controlled by the laser position, opening the door to mapping spatial effects of temperature on cell behaviour in a 3D environment.

5.3 Conclusions

We herein report a gold-nanoparticle crosslinked filamentous supramolecular and covalent double network hydrogel through the simultaneous photopolymerization of 1,2-dithiolane and norbornene on the various components. By varying the concentration of gold nanoparticles, tunable mechanical properties, conductive and photothermal properties within these hybrid hydrogels can be achieved. Cross-linking of the gold nanoparticles to the double network yields increased energy dissipation similar to stiff and tough tissues such as cartilage. Prior to photopolymerization the materials can be extruded thorugh a syringe and remained stable in buffered solution showing printability. Furthermore, these hydrogels showed excellent cycling of the photo-thermal effect due to the gold nanoparticles. Further harnessing the photothermal effect in the presence of MDA-MB-231-B1 cells, cell ablation can be executed in a spatial manner by tuning the laser dose and nanoparticle concentration. These nanocomposite materials provide new opportunities to use toughen supramolecular polymer materials while studying their cell behaviour under extreme thermal conditions in a local manner, and open the door for potential 3D applications in photothermal treatment of cancer.

References

(1) Kunwar, P.; Ransbottom, M. J.; Soman, P. Three-Dimensional Printing of Double-Network Hydrogels: Recent Progress, Challenges, and Future Outlook. *3D Printing and Additive Manufacturing* **2021**, *9* (5), 435.

(2) Muir, V. G.; Burdick, J. A. Chemically Modified Biopolymers for the Formation of Biomedical Hydrogels. *Chem Rev* **2021,** *121* (18), 10908.

(3) Yu, C.; Schimelman, J.; Wang, P.; Miller, K. L.; Ma, X.; You, S.; Guan, J.; Sun, B.; Zhu, W.; Chen, S. Photopolymerizable Biomaterials and Light-Based 3D Printing Strategies for Biomedical Applications. *Chem Rev* **2020,** *120* (19), 10695.

(4) Yu, H.; Gao, R.; Liu, Y.; Fu, L.; Zhou, J.; Li, L. Stimulus‐Responsive Hydrogels as Drug Delivery Systems for Inflammation Targeted Therapy. *Advanced Science* **2023**, 2306152.

(5) Sithole, M. N.; Mndlovu, H.; du Toit, L. C.; Choonara, Y. E. Advances in Stimuli-responsive Hydrogels for Tissue Engineering and Regenerative Medicine Applications: A Review Towards Improving Structural Design for 3D Printing. *Current Pharmaceutical Design* **2023** *13*, 10186.

(6) Green, J. J.; Elisseeff, J. H. Mimicking biological functionality with polymers for biomedical applications. *Nature* **2016,** *540* (7633), 386.

(7) Kyburz, K. A.; Anseth, K. S. Synthetic mimics of the extracellular matrix: how simple is complex enough? *Annals of biomedical engineering* **2015,** *43*, 489.

(8) Zhao, Z.; Chen, X.; Dowbaj, A. M.; Sljukic, A.; Bratlie, K.; Lin, L.; Fong, E. L. S.; Balachander, G. M.; Chen, Z.; Soragni, A. Organoids. *Nature Reviews Methods Primers* **2022,** *2* (1), 94.

(9) Chivers, P. R. A.; Smith, D. K. Shaping and structuring supramolecular gels. *Nat. Rev. Mater.* **2019,** *4* (7), 463.

(10) Tong, C.; Liu, T.; Saez Talens, V.; Noteborn, W. E.; Sharp, T. H.; Hendrix, M. M.; Voets, I. K.; Mummery, C. L.; Orlova, V. V.; Kieltyka, R. E. Squaramide-based supramolecular materials for three-dimensional cell culture of human induced pluripotent stem cells and their derivatives. *Biomacromolecules* **2018,** *19* (4), 1091.

(11) Hutmacher, D. W. Scaffolds in tissue engineering bone and cartilage. *Biomaterials* **2000,** *21* (24), 2529.

(12) Huang, X.; Li, J.; Luo, J.; Gao, Q.; Mao, A.; Li, J. Research progress on double-network hydrogels. *Adv. Healthc. Mater.* **2021,** *29*, 102757.

(13) Sun, W.; Xue, B.; Li, Y.; Qin, M.; Wu, J.; Lu, K.; Wu, J.; Cao, Y.; Jiang, Q.; Wang, W. Polymer-Supramolecular Polymer Double-Network Hydrogel. *Adv. Funct. Mater.* **2016,** *26* (48), 9044.

(14) Nakayama, A.; Kakugo, A.; Gong, J. P.; Osada, Y.; Takai, M.; Erata, T.; Kawano, S. High Mechanical Strength Double-Network Hydrogel with Bacterial Cellulose. *Adv. Funct. Mater.* **2004,** *14* (11), 1124.

(15) Chen, Q.; Chen, H.; Zhu, L.; Zheng, J. Fundamentals of double network hydrogels. *J Mater Chem B* **2015,** *3* (18), 3654.

(16) Nonoyama, T.; Gong, J. P. Double-network hydrogel and its potential biomedical application: A review. *Proc Inst Mech Eng H* **2015,** *229* (12), 853.

(17) Ni, X.; Xing, X.; Deng, Y.; Li, Z. Applications of Stimuli-Responsive Hydrogels in Bone and Cartilage Regeneration. *Pharmaceutics* **2023,** *15* (3), 982.

(18) Monemian, S.; Korley, L. T. Exploring the role of supramolecular associations in mechanical toughening of interpenetrating polymer networks. *Macromolecules* **2015,** *48* (19), 7146.

(19) Goor, O.; Hendrikse, S. I. S.; Dankers, P. Y. W.; Meijer, E. W. From supramolecular polymers to multi-component biomaterials. *Chem. Soc. Rev.* **2017,** *46* (21), 6621.

(20) Radvar, E.; Azevedo, H. S. Supramolecular Peptide/Polymer Hybrid Hydrogels for Biomedical Applications. *Macromol Biosci* **2019,** *19* (1), e1800221.

(21) Webber, M. J.; Appel, E. A.; Meijer, E. W.; Langer, R. Supramolecular biomaterials. *Nat. Mater.* **2016,** *15* (1), 13.
(22) Yang, L.; Tan, X.; Wang, Z.; Zhang, X. Supramolecular Polymers: Historical Development, Preparation, Characterization, and Functions. *Chem Rev* **2015,** *115* (15), 7196.
(23) Du, X.; Zhou, J.; Shi, J.; Xu, B. Supramolecular Hydrogelators and Hydrogels: From Soft Matter to Molecular Biomaterials. *Chem Rev* **2015,** *115* (24), 13165.
(24) Hafeez, S.; Decarli, M. C.; Aldana, A.; Ebrahimi, M.; Ruiter, F. A.; Duimel, H.; van Blitterswijk, C.; Pitet, L. M.; Moroni, L.; Baker, M. B. In Situ Covalent Reinforcement of a Benzene-1, 3, 5-Tricarboxamide Supramolecular Polymer Enables Biomimetic, Tough, and Fibrous Hydrogels and Bioinks. *Adv. Mater.* **2023,** *35* (35), 2301242.
(25) Li, H.; Wang, H.; Zhang, D.; Xu, Z.; Liu, W. A highly tough and stiff supramolecular polymer double network hydrogel. *Polymer* **2018,** *153*, 193.
(26) Elkhoury, K.; Russell, C. S.; Sanchez-Gonzalez, L.; Mostafavi, A.; Williams, T. J.; Kahn, C.; Peppas, N. A.; Arab-Tehrany, E.; Tamayol, A. Soft-nanoparticle functionalization of natural hydrogels for tissue engineering applications. *Adv. Healthc. Mater.* **2019,** *8* (18), 1900506.
(27) Tan, H.-L.; Teow, S.-Y.; Pushpamalar, J. Application of metal nanoparticle–hydrogel composites in tissue regeneration. *Bioengineering* **2019,** *6* (1), 17.
(28) Hasan, A.; Khattab, A.; Islam, M. A.; Hweij, K. A.; Zeitouny, J.; Waters, R.; Sayegh, M.; Hossain, M. M.; Paul, A. Injectable hydrogels for cardiac tissue repair after myocardial infarction. *Advanced Science* **2015,** *2* (11), 1500122.
(29) Viola, M.; Piluso, S.; Groll, J.; Vermonden, T.; Malda, J.; Castilho, M. The Importance of Interfaces in Multi-Material Biofabricated Tissue Structures. *Adv Healthc Mater* **2021,** *10* (21), e2101021.
(30) Sano, K.; Ishida, Y.; Aida, T. Synthesis of Anisotropic Hydrogels and Their Applications. *Angew Chem Int Ed Engl* **2018,** *57* (10), 2532.
(31) Han, L.; Yan, L.; Wang, M.; Wang, K.; Fang, L.; Zhou, J.; Fang, J.; Ren, F.; Lu, X. Transparent, Adhesive, and Conductive Hydrogel for Soft Bioelectronics Based on Light-Transmitting Polydopamine-Doped Polypyrrole Nanofibrils. *Chem. Mater.* **2018,** *30* (16), 5561.
(32) Xing, W.; Tang, Y. On mechanical properties of nanocomposite hydrogels: Searching for superior properties. *Nano Materials Science* **2021**, *4*, 83.
(33) Arno, M. C.; Inam, M.; Weems, A. C.; Li, Z.; Binch, A. L.; Platt, C. I.; Richardson, S. M.; Hoyland, J. A.; Dove, A. P.; O'Reilly, R. K. Exploiting the role of nanoparticle shape in enhancing hydrogel adhesive and mechanical properties. *Nature communications* **2020,** *11* (1), 1420.
(34) Chen, W.; Kouwer, P. H. Combining mechanical tuneability with function: biomimetic fibrous hydrogels with nanoparticle crosslinkers. *Adv. Funct. Mater.* **2021,** *31* (47), 2105713.
(35) Cui, Z.-K.; Kim, S.; Baljon, J. J.; Wu, B. M.; Aghaloo, T.; Lee, M. Microporous methacrylated glycol chitosan-montmorillonite nanocomposite hydrogel for bone tissue engineering. *Nature communications* **2019,** *10* (1), 3523.
(36) Kim, Y.-H.; Yang, X.; Shi, L.; Lanham, S. A.; Hilborn, J.; Oreffo, R. O.; Ossipov, D.; Dawson, J. I. Bisphosphonate nanoclay edge-site interactions facilitate hydrogel self-assembly and sustained growth factor localization. *Nature communications* **2020,** *11* (1), 1365.
(37) Rose, S.; Dizeux, A.; Narita, T.; Hourdet, D.; Marcellan, A. Time dependence of dissipative and recovery processes in nanohybrid hydrogels. *Macromolecules* **2013,** *46* (10), 4095.
(38) Meng, X.; Qiao, Y.; Do, C.; Bras, W.; He, C.; Ke, Y.; Russell, T. P.; Qiu, D. Hysteresis-Free Nanoparticle-Reinforced Hydrogels. *Adv. Mater.* **2022,** *34* (7), 2108243.

(39) Pafiti, K.; Cui, Z.; Adlam, D.; Hoyland, J.; Freemont, A. J.; Saunders, B. R. Hydrogel composites containing sacrificial collapsed hollow particles as dual action pH-responsive biomaterials. *Biomacromolecules* **2016,** *17* (7), 2448.
(40) Gao, G.; Du, G.; Sun, Y.; Fu, J. Self-healable, tough, and ultrastretchable nanocomposite hydrogels based on reversible polyacrylamide/montmorillonite adsorption. *ACS Appl. Mater. Interfaces* **2015,** *7* (8), 5029.
(41) Liu, X.; Miller, A. L., 2nd; Park, S.; Waletzki, B. E.; Zhou, Z.; Terzic, A.; Lu, L. Functionalized Carbon Nanotube and Graphene Oxide Embedded Electrically Conductive Hydrogel Synergistically Stimulates Nerve Cell Differentiation. *ACS Appl. Mater. Interfaces* **2017,** *9* (17), 14677.
(42) Min, J. H.; Patel, M.; Koh, W. G. Incorporation of Conductive Materials into Hydrogels for Tissue Engineering Applications. *Polymers (Basel)* **2018,** *10*, 1078.
(43) Thoniyot, P.; Tan, M. J.; Karim, A. A.; Young, D. J.; Loh, X. J. Nanoparticle-Hydrogel Composites: Concept, Design, and Applications of These Promising, Multi-Functional Materials. *Adv Sci (Weinh)* **2015,** *2* (1-2), 1400010.
(44) Dannert, C.; Stokke, B. T.; Dias, R. S. Nanoparticle-Hydrogel Composites: From Molecular Interactions to Macroscopic Behavior. *Polymers (Basel)* **2019,** *11*, 275.
(45) Chen, T.; Hou, K.; Ren, Q.; Chen, G.; Wei, P.; Zhu, M. Nanoparticle-Polymer Synergies in Nanocomposite Hydrogels: From Design to Application. *Macromol. Rapid Commun.* **2018,** *39* (21), e1800337.
(46) Elkhoury, K.; Russell, C. S.; Sanchez-Gonzalez, L.; Mostafavi, A.; Williams, T. J.; Kahn, C.; Peppas, N. A.; Arab-Tehrany, E.; Tamayol, A. Soft-Nanoparticle Functionalization of Natural Hydrogels for Tissue Engineering Applications. *Adv Healthc Mater* **2019,** *8* (18), e1900506.
(47) Tan, H. L.; Teow, S. Y.; Pushpamalar, J. Application of Metal Nanoparticle(-)Hydrogel Composites in Tissue Regeneration. *Bioengineering (Basel)* **2019,** *6,* 17.
(48) Dvir, T.; Timko, B. P.; Brigham, M. D.; Naik, S. R.; Karajanagi, S. S.; Levy, O.; Jin, H.; Parker, K. K.; Langer, R.; Kohane, D. S. Nanowired three-dimensional cardiac patches. *Nat Nanotechnol* **2011,** *6* (11), 720.
(49) Navaei, A.; Rahmani Eliato, K.; Ros, R.; Migrino, R. Q.; Willis, B. C.; Nikkhah, M. The influence of electrically conductive and non-conductive nanocomposite scaffolds on the maturation and excitability of engineered cardiac tissues. *Biomater Sci* **2019,** *7* (2), 585.
(50) Huang, X.; El-Sayed, M. A. Gold nanoparticles: Optical properties and implementations in cancer diagnosis and photothermal therapy. *Journal of Advanced Research* **2010,** *1* (1), 13.
(51) Wahid, F.; Zhao, X.-J.; Jia, S.-R.; Bai, H.; Zhong, C. Nanocomposite hydrogels as multifunctional systems for biomedical applications: Current state and perspectives. *Composites Part B: Engineering* **2020,** *200*.
(52) Tong, C.; Wondergem, J. A. J.; van den Brink, M.; Kwakernaak, M. C.; Chen, Y.; Hendrix, M.; Voets, I. K.; Danen, E. H. J.; Le Devedec, S.; Heinrich, D.et al. Spatial and Temporal Modulation of Cell Instructive Cues in a Filamentous Supramolecular Biomaterial. *ACS Appl. Mater. Interfaces* **2022,** *14* (15), 17042.
(53) Tong, C.; Wondergem, J. A. J.; Heinrich, D.; Kieltyka, R. E. Photopatternable, Branched Polymer Hydrogels Based on Linear Macromonomers for 3D Cell Culture Applications. *ACS Macro Lett.* **2020,** *9* (6), 882.
(54) John Turkevich, P. C. S., James Hillie. A study of the nucleation and growth processes in the synthesis of colloidal gold. *Synthesis Of Colloidal Gold* **1951**, 55.
(55) Frens., G. Controlled Nucleation for the Regulation of the Particle Size in Monodisperse Gold Suspensions. *Nature Physical Science* **1973,** *241(105)*, 20.
(56) Pacchioni, G. A not-so-strong bond. *Nature Reviews Materials* **2019,** *4* (4), 226.
(57) Bard, A.; Rondon, R.; Marquez, D. T.; Lanterna, A. E.; Scaiano, J. C. How Fast Can Thiols Bind to the Gold Nanoparticle Surface? *Photochem. Photobiol.* **2018,** *94* (6), 1109.
(58) Dannert, C.; Stokke, B. T.; Dias, R. S. Nanoparticle-hydrogel composites: from molecular interactions to macroscopic behavior. *Polymers* **2019,** *11* (2), 275.

(59) Bapat, R. A.; Chaubal, T. V.; Dharmadhikari, S.; Abdulla, A. M.; Bapat, P.; Alexander, A.; Dubey, S. K.; Kesharwani, P. Recent advances of gold nanoparticles as biomaterial in dentistry. *Int. J. Pharm.* **2020,** *586*, 119596.
(60) Yadid, M.; Feiner, R.; Dvir, T. Gold nanoparticle-integrated scaffolds for tissue engineering and regenerative medicine. *Nano Lett.* **2019,** *19* (4), 2198.
(61) Jaiswal, M. K.; Xavier, J. R.; Carrow, J. K.; Desai, P.; Alge, D.; Gaharwar, A. K. Mechanically stiff nanocomposite hydrogels at ultralow nanoparticle content. *ACS nano* **2016,** *10* (1), 246.
(62) Gaharwar, A. K.; Dammu, S. A.; Canter, J. M.; Wu, C.-J.; Schmidt, G. Highly extensible, tough, and elastomeric nanocomposite hydrogels from poly (ethylene glycol) and hydroxyapatite nanoparticles. *Biomacromolecules* **2011,** *12* (5), 1641.
(63) Murphy, C. M.; O'Brien, F. J. Understanding the effect of mean pore size on cell activity in collagen-glycosaminoglycan scaffolds. *Cell adhesion & migration* **2010,** *4* (3), 377.
(64) Loh, Q. L.; Choong, C. Three-dimensional scaffolds for tissue engineering applications: role of porosity and pore size. **2013**, 19, 485.
(65) Tong, C.; Liu, T.; Saez Talens, V.; Noteborn, W. E. M.; Sharp, T. H.; Hendrix, M.; Voets, I. K.; Mummery, C. L.; Orlova, V. V.; Kieltyka, R. E. Squaramide-Based Supramolecular Materials for Three-Dimensional Cell Culture of Human Induced Pluripotent Stem Cells and Their Derivatives. *Biomacromolecules* **2018,** *19* (4), 1091.
(66) Park, H.; Guo, X.; Temenoff, J. S.; Tabata, Y.; Caplan, A. I.; Kasper, K.; Mikos, A. G. Effect of Swelling Ratio of Injectable Hydrogel Composites on Chondrogenic Differentiation of Encapsulated Rabbit Marrow Mesenchymal Stem Cells *In Vitro*. *Biomacromolecules* **2009,** *10*, 541.
(67) Miao, Z.; Gao, Z.; Chen, R.; Yu, X.; Su, Z.; Wei, G. Surface-bioengineered gold nanoparticles for biomedical applications. *Current Medicinal Chemistry* **2018,** *25* (16), 1920.
(68) Jiang, J.; Xu, S.; Ma, H.; Li, C.; Huang, Z. Photoresponsive hydrogel-based soft robot: A review. *Materials Today Bio* **2023**, 100657.
(69) Cabuzu, D.; Cirja, A.; Puiu, R.; Mihai Grumezescu, A. Biomedical applications of gold nanoparticles. *Curr. Top. Med. Chem.* **2015,** *15* (16), 1605.
(70) Xu, Y.; Rothe, R.; Voigt, D.; Hauser, S.; Cui, M.; Miyagawa, T.; Patino Gaillez, M.; Kurth, T.; Bornhäuser, M.; Pietzsch, J. Convergent synthesis of diversified reversible network leads to liquid metal-containing conductive hydrogel adhesives. *Nature communications* **2021,** *12* (1), 2407.
(71) Rengan, A. K.; Jagtap, M.; De, A.; Banerjee, R.; Srivastava, R. Multifunctional gold coated thermo-sensitive liposomes for multimodal imaging and photo-thermal therapy of breast cancer cells. *Nanoscale* **2014,** *6* (2), 916.
(72) Zhi, D.; Yang, T.; O'hagan, J.; Zhang, S.; Donnelly, R. F. Photothermal therapy. *J. Controlled Release* **2020,** *325*, 52.
(73) Hussein, E. A.; Zagho, M. M.; Nasrallah, G. K.; Elzatahry, A. A. Recent advances in functional nanostructures as cancer photothermal therapy. *International journal of nanomedicine* **2018**, 2897.
(74) Liu, S.; Pan, X.; Liu, H. Two‐dimensional nanomaterials for photothermal therapy. *Angew. Chem.* **2020,** *132* (15), 5943.
(75) Wu, Y.; Wang, H.; Gao, F.; Xu, Z.; Dai, F.; Liu, W. An Injectable Supramolecular Polymer Nanocomposite Hydrogel for Prevention of Breast Cancer Recurrence with Theranostic and Mammoplastic Functions. *Adv. Funct. Mater.* **2018,** *28*, 1801000.
(76) Hwang, S.; Nam, J.; Jung, S.; Song, J.; Doh, H.; Kim, S. Gold nanoparticle-mediated photothermal therapy: current status and future perspective. *Nanomedicine* **2014,** *9* (13), 2003.

(77) Yang, W.; Liang, H.; Ma, S.; Wang, D.; Huang, J. Gold nanoparticle based photothermal therapy: Development and application for effective cancer treatment. *Sustainable Materials and Technologies* **2019,** *22*, e00109.
(78) Riley, R. S.; Day, E. S. Gold nanoparticle‐mediated photothermal therapy: applications and opportunities for multimodal cancer treatment. *Wiley Interdisciplinary Reviews: Nanomedicine and Nanobiotechnology* **2017,** *9* (4), e1449.

Supporting information

S5.1 Materials and methods

Materials

SH-PEG_{5400}-NH_2 (Mw: 5 kDa) and SH-PEG_{5000} (Mw: 5 kDa) was obtained from Iris Biotech. 4 arm-PEG-OH (Mw: 10 kDa) from Jenkem Technology. Deuterated solvents for NMR experiments were obtained from Euriso-top. Formvar/Carbon 200 mesh copper grid and lacey carbon 200 mesh grids were purchased from Electron Microscopy Sciences. Dulbecco's phosphate buffered saline (DPBS, pH=7.4) was purchased from Sigma Aldrich. Dulbecco's modified Eagle medium (DMEM), antibiotics penicillin and streptomycin were received from Gibco, Life Technologies. Fetal bovine serum (FBS) was produced from Biowest. The antibiotics penicillin and streptomycin were purchased from Gibco. Collagenase Type I was obtained from Worthington Biochemical Corporation. µ-Slide 8 Well and 15 Well 3D chambered coverplates were purchased from Ibidi. **C8-SQ** (**4**) and **C8-SQ-DT** (**5**) were synthesized as previous reported.[1,2] N-hydroxysuccinimide, N,N'-dicyclohexylcarbodiimide and all other commercially available chemicals were purchased from Sigma Aldrich at the highest purity available and used without further purification. Milli-Q water was employed for all the experiments. All reaction vessels for gold nanoparticles synthesis were washed carefully with aqua regia before use. Gold nanoparticles was stored at -4°C and the rest compounds were stored at -20°C for further usage.

Methods

^{1}H-NMR and ^{13}C-NMR spectra were recorded on a Bruker DMX-400. All supramolecular monomers were purified by high performance liquid chromatography (HPLC) on a Shimadzu system equipped with two LC-20AR pumps, an SPD-20A UV-Vis detector and Phenomenex Kinetex EVO C18 column. The mobile phases were CH_3CN and H_2O with 0.1% trifluoroacetic acid. Liquid chromatography-mass spectrometry (LC-MS) analysis was performed on a Finnigan Surveyor HPLC system equipped (UV detection from 200-600 nm) with a Gemini C18 50 x 4.60 mm reverse phase column coupled to Finnigan LCQ Advantage Max mass spectrometer with ESI. For the mobile phase, a gradient of 10-90% of CH_3CN/H_2O with 0.1% trifluoroacetic acid over 13.5 minutes was used. UV absorption spectra were acquired at room temperature (RT) on a Cary 300 UV-Vis spectrophotometer from 400 to 800 nm using a quartz cuvette with a path length of 1 cm. The hydrodynamic diameter and zeta potential tests were performed on Malvern Zetasizer Nano S. Oscillatory rheology experiments were performed on a Discovery Hybrid Rheometer (DHR-2) from TA Instruments with a Smart Swap UV assembly with a quartz lower plate (20 mm) and a aluminum upper plate (8 mm) at RT using a fixed gap of 300 µm, UV light (λ = 320-500 nm, primary peak: 365 nm) was applied through an Omnicure S2000 high-pressure mercury light source from Excelitas connected to the rheometer through a light guide (5 mm diameter). The UV intensity was calibrated using a Silverline radiometer sensor (20 mm) accessory designed for the quartz parallel plate. The compressive properties were assessed under the same conditions on DHR-2 at a fixed gap of 1 mm and a maximum axial force of 50 N. The diameters and of the gold nanoparticles were imaged on a JEOL JEM-1400 Plus transmission electron microscope (TEM). The distributions of gold nanoparticles in the **DN** and **DN-Au** hydrogels were imaged on TEM and cryogenic electron

microscope (cryo-EM) on a Talos L120C operating at 120 kV, samples were plunge frozen on a Vitrobot Mark IV, both from Thermo Fisher Scientific. The surface morphology and pore sizes of the lyophilized hydrogels were imaged by scanning electron microscope (SEM) using a JSM-7600F microscope from JEOL under high vacuum with an acceleration voltage of 2.0 kV. The conductivity measurement was assessed using a Metrohm Autolab Potentiostat by scanning from 1 MHz to 1 Hz in 10 frequency measurement points per at 0 V to prevent localized oxidation. Photo-thermal effect was accessed by using Lighthouse Photonics Sprout laser at 532 nm and K-Type Digital Thermometer. Cells were cultured in Dubecco's modified Eagle medium (DMEM) with high glucose, with 10% fetal calf serum, 0.1% glutamax, 0.2% penicillin and 0.2% streptomycin. Images for cell viability assessment in 3D cultures were captured on a Stellaris 8 confocal laser scanning microscope from Leica with a supercontinuum white light laser (440-790 nm) and Power HyD detectors, the excitation wavelengths of 486 nm (Calcein AM) and 532 nm (propidium iodide), and emission filters of 500-545 nm (Calcein AM) and 594-686 nm (propidium iodide) were used, respectively. Live and dead cells were counted using a Fiji/ImageJ macro written for 3D analysis of LIVE/DEAD cells. The confocal pictures were processed using Fiji/ImageJ software. A benchtop LED light (~10 mW/cm², 375 nm) was employed to initiate crosslinking in all other samples except for the ones on the rheometer.

Experimental Details

Synthesis of hydrogel components

DT (1)

4-methyl-1,2-dithiolane-4-carboxylic acid (**DT**) was synthesized as reported before.[1,3] Briefly, 3,3-Dichloropivalic acid (2.00 g, 11.69 mmol) and water (15 mL) were mixed in a 3-neck round bottom flask. Sodium carbonate (1.14 g, 10.76 mmol) was added slowly. When 3,3 dichloropivalic acid was fully dissolved under stirring, an aqueous solution (5 mL) containing potassium thioacetate (2.71 g, 23.64 mmol) was added dropwise over a period of a few minutes. The solution was then heated to 100 °C and refluxed for 8 h. Then, sodium carbonate (3.84 g, 35.85 mmol) was added slowly, and the yellow solution turned green, then yellow again after a few minutes. After disappearance of the starting material, dimethyl sulfoxide (DMSO, 1.8 mL) was added, and the solution was refluxed for another 8 h at 100 °C. The reaction mixture was cooled to RT and acidified with 1 M hydrochloric acid. A yellow precipitate was collected, washed with ice-cold water and dried in an oven overnight at 60 °C. Yield: 660 mg, 34%. ^{1}H-NMR (400 MHz, DMSO-D_6): 3.59 (s, 1H), 3.56 (s, 1H), 3.01 (s, 1H), 2.98 (s, 1H), 1.40 (s, 3H). ^{13}C-NMR (DMSO-D_6, 100 MHz): 170.43, 55.53, 45.62, 22.13.

HS-PEG$_{5400}$-DT (2)

1,2-Dithiolane-3-carboxylic acid (500.00 mg, 3.00 mmol), N,N'-dicyclohexylcarbodiimide (DCC) (618.99 mg, 3.00 mmol) and N-hydroxysuccinimide (NHS) (350.00 mg, 3.00 mmol) were dissolved in dry CH_2Cl_2 (10 mL). The reaction was stirred overnight at RT under nitrogen gas. The reaction mixture was collected and filtered twice, and the filtrate was dried on a rotary evaporator at 40 °C under vacuum (700 mbar) to get a light-yellow compound (DT-NHS). Afterwards, to a stirring solution of HS-PEG$_{5400}$-NH_2 (200.00 mg, 0.04 mmol) solution in dry CH_2Cl_2 (5 mL), DT-NHS (79.30 mg, 0.19 mmol) and DIPEA (63.34 µL, 0.37 mmol) were added and reacted

overnight under nitrogen gas. The mixed solution was filtered and concentrated by a stream of nitrogen gas before being precipitated in cold diethyl ether, washed and re-dissolved in CH_2Cl_2 (10 mL). The precipitation step was repeated 3 times, then H_2O (2 mL) was added to dissolve the obtained solid and the product was lyophilized overnight to obtain a white solid. Yield: 186 mg, 90%. ^{1}H-NMR (400 MHz, $CDCl_3$): 3.47-3.84 (m, 486H), 3.31-3.33 (t, 4H), 2.99-3.02 (d, 2H), 2.49-2.51 (t, 2H), 2.95 (s, 3H).

PEG4-NB

To a stirring solution of 5-norbornene-2-carboxylic acid (**NB**, 183.63 µL, 1.50 mmol) in dry CH_2Cl_2 (5 mL), DCC (309.51 mg, 1.50 mmol) was added and the mixture was kept at RT for 30 min. Subsequently, the reaction mixture was added to a solution (5 mL) containing 4-arm polyethylene glycol (Mw: 10 kDa) (500 mg, 0.05 mmol), pyridine (40.23 µL, 0.50 mmol) and 4-dimethylaminopyridine (DMAP, 12.22 mg, 0.10 mmol), and stirred overnight at RT. The mixed solution was filtered and concentrated by a stream of nitrogen gas before being precipitated in cold diethyl ether, washed and re-dissolved in CH_2Cl_2 (10 mL). The precipitation step was repeated 3 times, then H_2O (2 mL) was added to dissolve the obtained solid and dialyzed for 3 days. The product was lyophilized overnight to obtain a white solid. Yield: 494 mg, 94%. ^{1}H-NMR (400 MHz, $CDCl_3$): 5.94-6.21 (m, 8H), 4.16-4.28 (m, 8H), 3.47-3.85 (m, 909H).

PEG4-DT

To a stirring solution of **DT** (131.00 mg, 0.80 mmol) in dry CH_2Cl_2 (5 mL), DCC (165.06 mg, 0.80 mmol) was added and the mixture was reacted at RT for 30 min. Subsequently, the reaction mixture was added to a solution (5 mL) containing 4-arm polyethylene glycol (Mw: 10 kDa) (500 mg, 0.05 mmol), pyridine (40.23 µL, 0.50 mmol) and 4-dimethylaminopyridine (DMAP, 12.22 mg, 0.10 mmol), and stirred overnight at RT. The reaction mixture was filtered and concentrated by a stream of nitrogen gas before being precipitated in cold diethyl ether, washed and re-dissolved in CH_2Cl_2 (10 mL). The precipitation step was repeated 3 times, then H_2O (2 mL) was added to dissolve the obtained solid and dialyzed for 3 days. The product was lyophilized overnight to obtain a white solid. Yield: 487.6 mg, 87%. ^{1}H-NMR (400 MHz, $CDCl_3$): 4.32-4.33 (m, 8H), 3.83-3.85 (m, 8H), 3.74-3.69 (d, 8H), 3.48-3.67 (m, 961H), 3.43 (s, 8H), 2.95-2.98 (d, 8H), 1.51 (s, 12H).

Au@Citrate

Gold nanoparticles (15 nm) were synthesized following the methods of Turkevich and French.[4,5] Milli-Q water (24 mL) was refluxed and stirred in a 3-neck round bottom flask. A chloroauric acid ($HAuCl_4$) solution (25.4 mM, 985 µL) was added and kept boiling for 3 min, followed by a 1% wt. trisodium citrate dehydrate solution (5 mL). The mixture was refluxed for 30 min, during which the color of the solution turned from yellow to transparent to greyish/violet and then to deep red. The reaction mixture was cooled to RT, washed 2 times with Milli-Q water (12000 rpm, 40 min) and concentrated before usage.

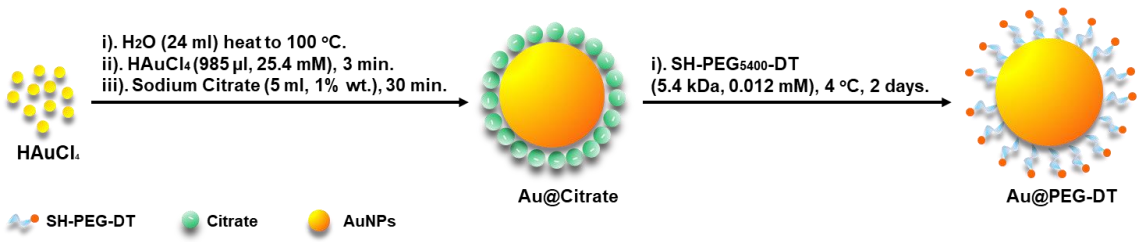

Figure S1. Synthesis route of **Au@Citrate** and **Au@PEG-DT**.

Au@PEG-DT

Au@PEG-DT nanoparticles were prepared by a ligand exchange reaction on gold.[6] Briefly, to an aqueous solution of **Au@Citrate** nanoparticles (10 mL, approximately 0.005 mM), **2** (60 mg, 0.012 mM) was added. The reaction was incubated for 3 days in the dark at 4 °C on a peptideshaker. The nanoparticles solution was washed 3 times by Milli-Q water to remove the excess ligand (12000 rpm, 40 min) and concentrated before usage. The concentration of **Au@PEG-DT** was obtained by ICP-MS.

Au@PEG

Au@PEG nanoparticles were prepared the same process as **Au@PEG-DT**, here we used SH-PEG_{5000} instead of **HS-PEG_{5400}-DT.**

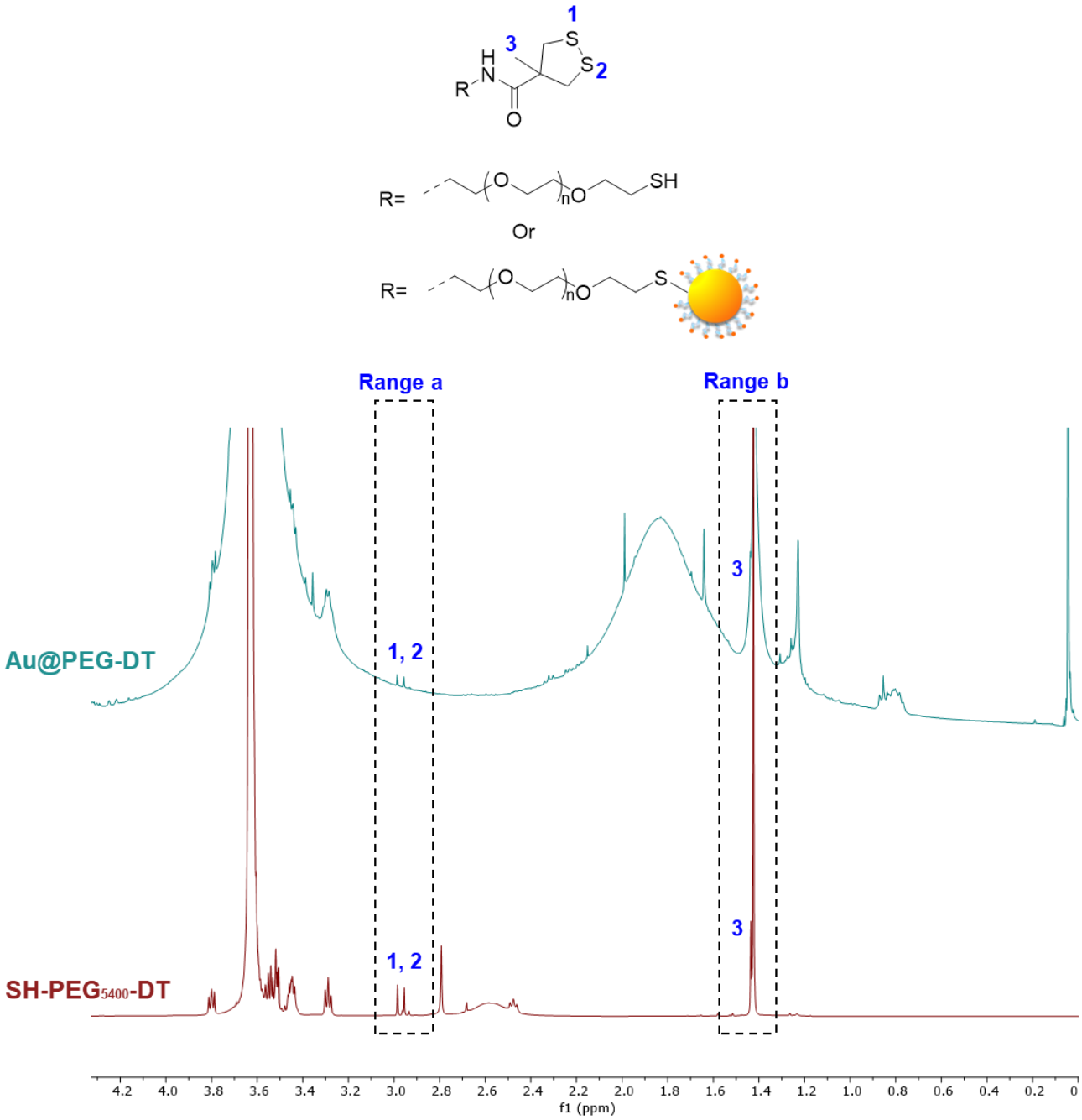

Figure S2. ^{1}H-NMR (400 Hz, 298K, $CDCl_3$) comparation spectrum of **Au@PEG-DT**(blue) and **HS-PEG$_{5400}$-DT**(red).

DLS and Zeta potential measurements

Au@Citrate (~1 mM) and **Au@PEG-DT** (~0.8 mM) solutions in Milli-Q water were prepared and measured at 25 °C. The hydrodynamic diameter and zeta potential was based on average of 5 measurements.

UV-Vis spectroscopy

Au@Citrate (~1 mM), **Au@PEG-DT** (0.8 mM) and **Au@PEG** (~0.8 mM) solutions in Milli-Q water were prepared after synthesis to obtain the UV spectra. The individual samples were left to equilibrate for 2 min at RT prior to measurements.

Transmission electron microscopy (TEM)

Aqueous gold nanoparticle solutions (5 µL, 300 ug/ml) in Milli-Q water were drop-casted on a Formvar/Carbon 200 mesh copper grid and dried at RT overnight before imaging.

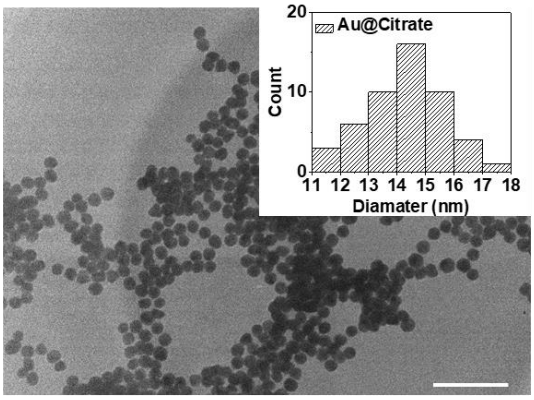

Figure S3. TEM picture of **Au@Citrate** (300 µg/ml). Insert: size distribution of AuNPs. Scale bar: *100 nm*.

Multicomponent hydrogels preparation

First, stock solutions of **C8-SQ** (10 mM) and **C8-SQ-DT** (10 mM) were prepared separately by dissolving the compounds in DMSO with 3 min of vortexing. To acquire **C8-SQ/10C8-SQ-DT** (10 molar percentages of **C8-SQ-DT** of the total monomer concentration) hydrogels (100 µL, 8 mM), **C8-SQ** (72 µL) and **C8-SQ-DT** (8 µL) stock solutions were pipetted into the glass vials (2.0 mL) with 1 min of gentle vortexing. Subsequently, the solutions were dried overnight under a stream of nitrogen gas. Water (100 µL) was added to the film of supramolecular monomers to prepare a hydrogel at final monomer concentration of 8 mM. Sonication was performed in an ice bath yielding a clear solution. To prepare the double network with gold nanoparticles, **PEG$_4$-NB** (10 wt%), **PEG$_4$-DT** (10 wt%) and **Au@PEG-DT** (7.68 mg/mL) or **Au@PEG** (6.8 mg/mL) solutions were added to the solution of supramolecular and left overnight equilibration. Lithium Phenyl(2,4,6-trimethylbenzoyl)phosphinate (LAP, 20 mM) was mixed with the **DN** hydrogel before crosslinking. The hydrogels without and with **Au@PEG-DT** were called **DN** and **DN-Au**, respectively. The hydrogels with 0.25 mg/mL **Au@PEG** were called **DN-Au@PEG$_{0.25}$**. For all the **DN**, **DN-Au** and **DN-Au@PEG$_{0.25}$** hydrogels in this paper, the final concentration of supramolecular hydrogel was 4 mM, LAP was 1 mM, functionalized group of **PEG$_4$-NB** and **PEG$_4$-DT** were 1.5 mM, respectively. **Au@PEG-DT** concentration was varied from 0.1 mg/mL to 1 mg/mL to obtain different **DN-Au** hydrogels, namely, **DN-Au$_x$** (**x** mg/mL **Au@PEG-DT** in the hydrogel). For example, to prepare **DN-Au$_{0.25}$** (100 µL), 14.49 µL Milli Q water, 15.96 µL **PEG$_4$-NB** (10 wt%), 16.30 µL **PEG$_4$-DT** (10 wt%) and 3.25 µL **Au@PEG-DT (**7.68 **mg/mL)** were added into 50 µL **C8-SQ/10C8-SQ-DT** (8 mM), evenly mixed by pipetted 10 times and left overnight equilibration to allow gelation to occur. 5 µL LAP (20 mM) was added and pipetted 10 times prior to other measurements. The uncross-linked gelation protocol was

utilized for all hydrogels discussed in this paper, with the exception of those that were specially illustrated.

Gel inversion test

For gel inversion tests, **DN** and **DN-Au** hydrogels (100 µL) were prepared in glass vials (2 mL) and crosslinked with a LED for 10 min. Milli-Q water (150 µL) was layered on top of each hydrogel and replaced every 2 days. Digital photos were taken on Day 0 before and after crosslinking and on Day 15 at the end of the experinment.

Figure S4. Gel inversion test before and after UV irradiation at Day 0 and at Day 15 at the end of the experiment.

Oscillatory rheology

DN and **DN-Au** hydrogels were prepared according to previously established uncross-linked gelation protocol, and gently pipetted on to the quartz plate under a fixed gap at 0.7 mm. Before data collection, the loaded samples were equilibrated for 5 min to allow the hydrogels to self-recover. After a time sweep experiment for 60 s, the hydrogels were stiffened by applying a UV light for 10 min. All the oscillatory time sweeps were performed at a strain amplitude (γ) of 0.05% and a frequency (ƒ) of 1 Hz. Frequency sweeps were assessed in a frequency range of 0.01 Hz to 10 Hz at a constant strain amplitude (γ = 0.05%). Strain sweeps were performed in a range of strain amplitudes of 0.01 % to 1000 % at a fixed frequency (ƒ = 1.0 Hz).

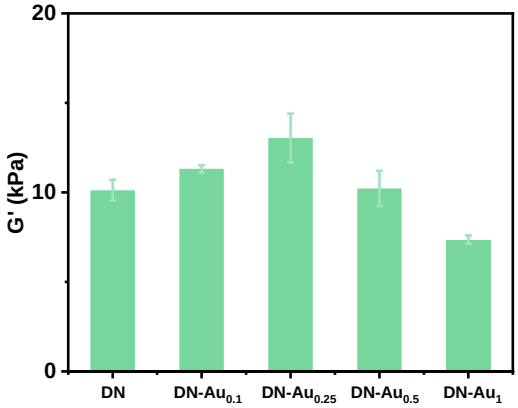

Figure S5. Plateau storage moduli (G') of photo-crosslinked **DN** and **DN-Au** hydrogels in Milli Q water at RT. Mean ± SD, N≥3.

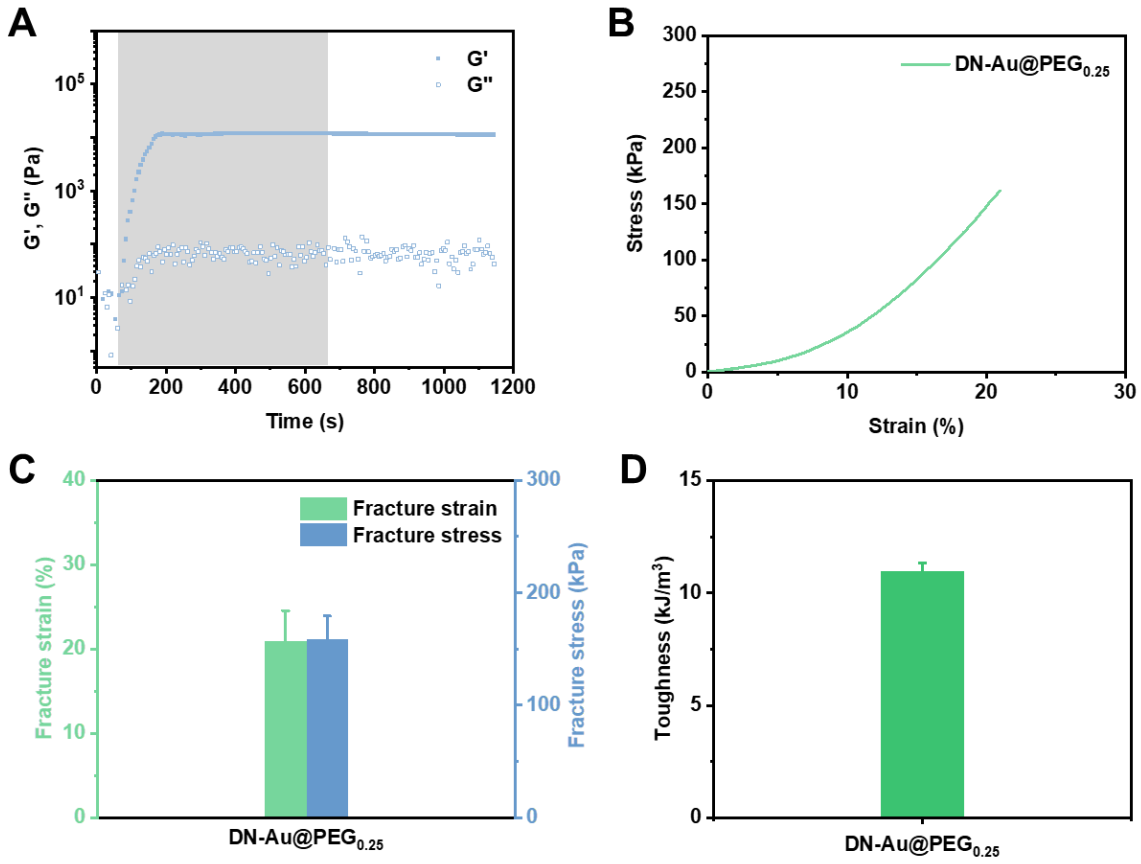

Figure S6. Mechanical properties **DN-Au@PEG$_{0.25}$** hydrogel: (A) Time sweep measurements of hydrogel before/after 10 min UV irradiation using a fixed strain (γ = 0.05%) and frequency (ƒ = 1.0 Hz) at room temperature. Grey regions indicate UV exposure. (B) Compression stress-strain response of UV crosslinked **DN-Au@PEG$_{0.25}$** hydrogel under a constant compression speed (10 µm/s) for 80 s at room temperature. (C) Compressive fracture strain and compressive fracture stress of UV crosslinked **DN-Au@PEG$_{0.25}$** hydrogel under a constant compression speed (10 µm/s). Mean ± SD, N≥3. (D). Compressive toughness of UV crosslinked **DN-Au@PEG$_{0.25}$** hydrogel under a constant compression speed (10 µm/s). Mean ± SD, N ≥ 3.

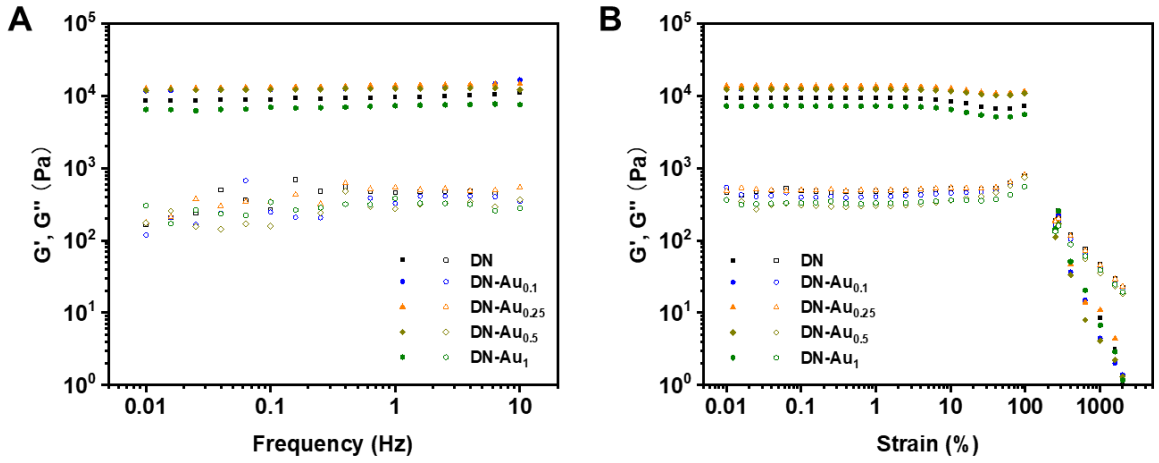

Figure S7. Oscillatory rheology measurements of UV crosslinked **DN** and **DN-Au** hydrogels in Milli Q water at RT: (A) Frequency sweep (γ = 0.05%). (B) Amplitude sweep (ƒ = 1.0 Hz).

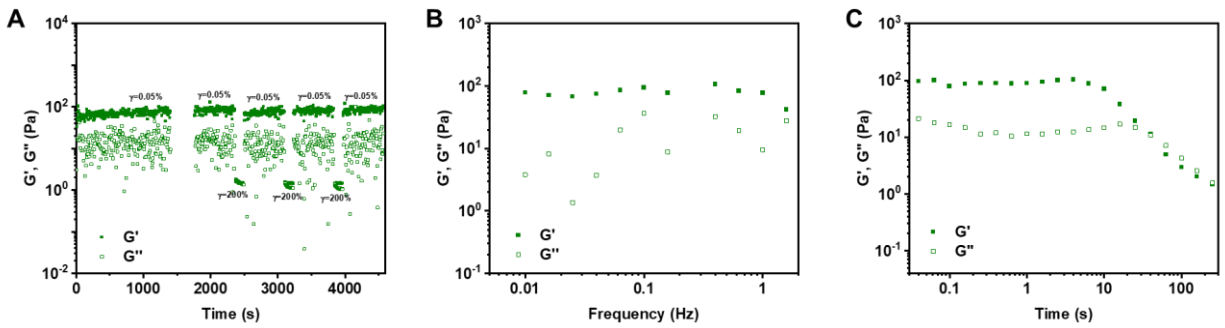

Figure S8. Oscillatory rheology measurements of **DN-Au$_{0.25}$** hydrogel in MilliQ water at RT: (A) Time sweep measurements (ƒ = 1 Hz, γ = 0.05%) and self-recovery process. The absence of data prior to applying a high strain (200%) can be attributed to conducting a frequency sweep prior to the measurement (ƒ = 0.01 to 2 Hz, γ = 0.05%). (B) Frequency sweep (γ = 0.05%). (C) Amplitude sweep (ƒ = 1 Hz).

Compression study

DN and **DN-Au** hydrogels were prepared according to previously established uncross-linked gelation protocol, and gently pipetted on to the quartz plate of the rheometer and the upper plate was lowered to 1 mm, equilibrated for 5 min before data collection. After a time sweep experiment for 60 s, the samples were irradiated with UV light for 10 min to reach a plateau in storage modulus. Subsequently, an axial experiment was set up compressing the sample to 50% of its initial height (500 µm gap) with a constant speed of 10 µm/s. Energy dissipation within the photocrosslinked gels were probed under the same conditions as the cyclic axial compression test using increasing strain percentages from 5% to 25% at a speed of 10 µm/s. The normal stress was plotted versus Cauchy strain (or engineering strain, the change in gap percentage as measured with respect to its initial setting) to get the compression curves of the hydrogels. The compressive fracture strain or stress was defined as the strain or stress at the breaking point. Toughness was calculated by the area under the stress-strain curve up to the point of fracture. The cyclic hysteresis curves were plotted as the compression curves before fracture. The dissipated energy was estimated by the area between loading - unloading curves.

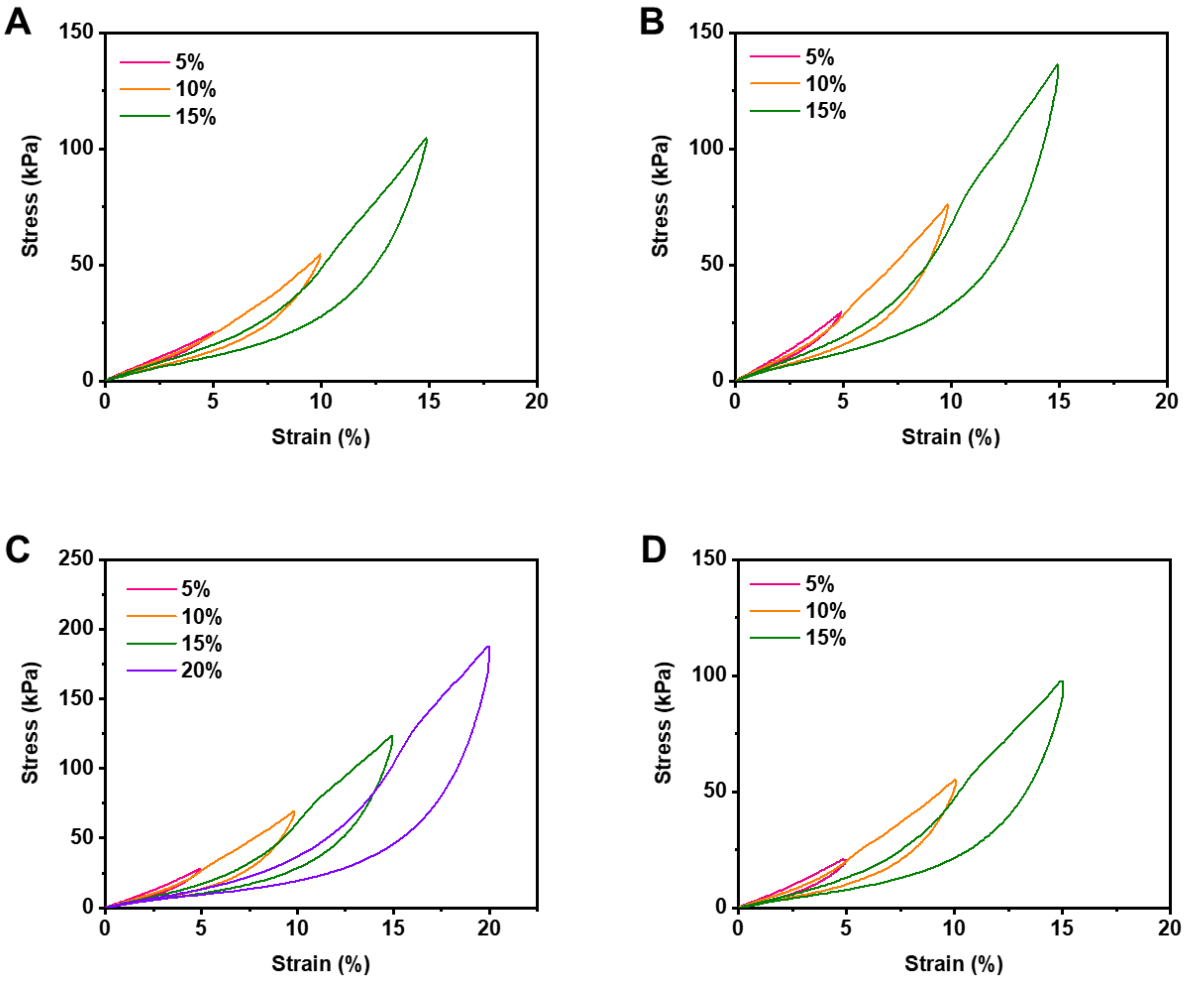

Figure S9. Cyclic hysteresis curves of UV crosslinked **DN** and **DN-Au** hydrogels at different maximum strains (λ_{max}) using a loading - unloading test under a constant compression speed (10 µm/s) at RT before break: (A) **DN**, (B) **DN-Au$_{0.1}$**, (C) **DN-Au$_{0.5}$**, (D) **DN-Au$_{1}$**.

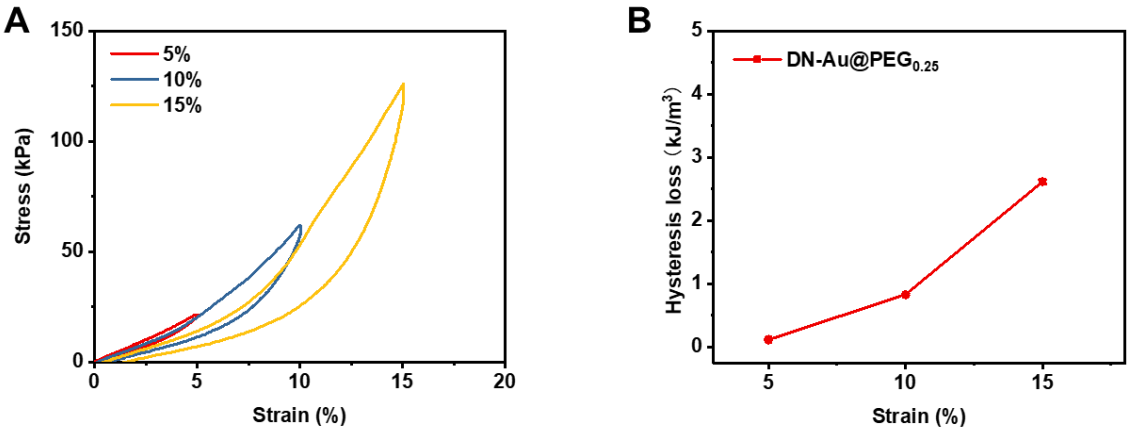

Figure S10. Mechanical properties **DN-Au@PEG$_{0.25}$** hydrogel: (A) Cyclic hysteresis curves of UV photocrosslinked hydrogel at different maximum strains (λ_{max}) using a loading - unloading test under a constant compression speed (10 µm/s) at RT before break. (B) Hysteresis loss of photocrosslinked hydrogel. Mean ± SD, N ≥ 3.

(Cryogenic) Transmission Electron microscopy ((Cryo)-TEM)

DN and **DN-Au** hydrogels (100 µL) were prepared according to previously established uncross-linked gelation protocol. The hydrogels were then diluted (10 times) to obtain their respective measured concentrations (0.4 mM of **C8-SQ/10C8-SQ-DT**, 0.15 mM NB of **PEG$_4$-NB**, 0.15 mM DT of **PEG$_4$-NB**, 0 mg/mL - 0.05 mg/mL of **Au@PEG-DT** and 0.1 mM LAP), and exposed to a LED for 10 min. Solution (10 µL) was carefully placed on Formvar/Carbon 200 mesh copper grid for 2 min and was removed by a paper, then uranyl acetate (10 µL, 1 %) was blotted on grid for 1 min and was removed by a paper. The grid was dried overnight at RT before imaging. The diameters of the gold nanostructures were measured manually in Fiji/ImageJ.

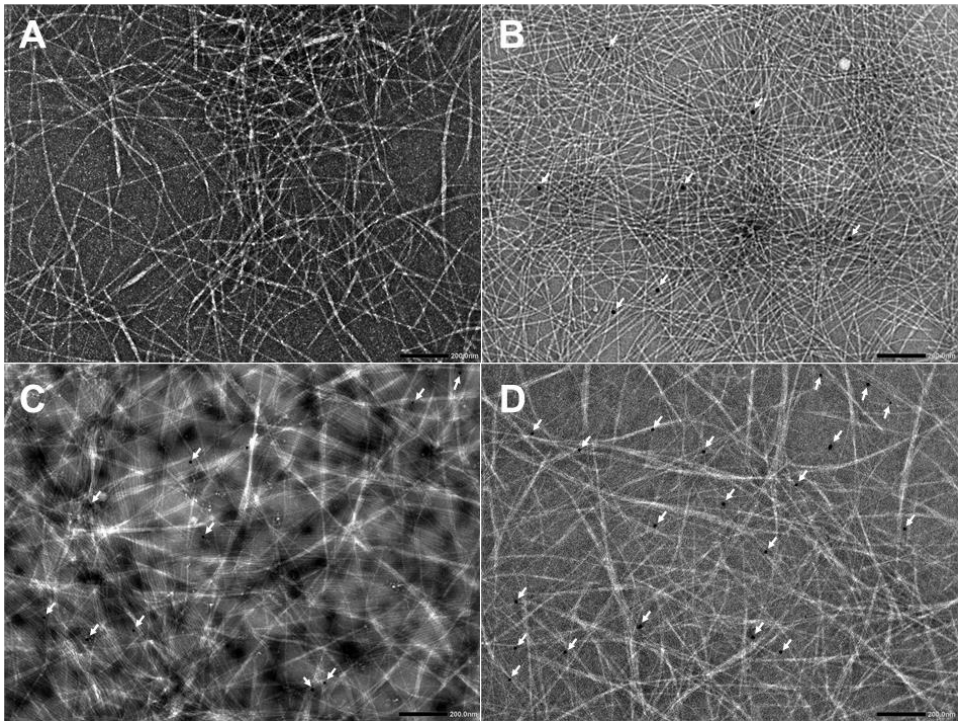

Figure S11. TEM images of diluted **DN** and **DN-Au** hydrogels after UV crosslinking: (A) **DN** (0.4 mM of **C8-SQ/10C8-SQ-DT**, 0.15 mM NB of **PEG$_4$-NB**, 0.15 mM DT of **PEG$_4$-DT**). (B) **DN-Au$_{0.1}$** (0.4 mM of **C8-SQ/10C8-SQ-DT**, 0.15 mM NB of **PEG$_4$-NB**, 0.15 Mm DT of **PEG$_4$-DT**, 0.01 mg/mL of **Au@PEG-DT**). (C) **DN-Au$_{0.25}$** (0.4 mM of **C8-SQ/10C8-SQ-DT**, 0.15 mM NB of **PEG$_4$-NB**, 0.15 mM DT of **PEG$_4$-DT**, 0.025 mg/mL of **Au@PEG-DT**). (D) **DN-Au$_{0.5}$** (0.4 mM of **C8-SQ/10C8-SQ-DT**, 0.15 mM NB of **PEG$_4$-NB**, 0.15 mM DT of **PEG$_4$-DT**, 0.05 mg/mL of **Au@PEG-DT**). Scale bar: *200 nm*.

DN-Au$_{0.25}$ and **DN-Au$_{0.5}$** hydrogels (100 µL) were prepared according to previously established uncross-linked gelation protocol. The hydrogels were then diluted (10 times) to obtain diluted **DN-Au$_{0.25}$** (0.4 mM of **C8-SQ/10C8-SQ-DT**, 0.15 mM NB of **PEG$_4$-NB**, 0.15 Mm DT of **PEG$_4$-DT**, 0.025 mg/mL of **Au@PEG-DT** and 0.1 mM LAP) and **DN-Au$_{0.5}$** hydrogels (0.4 mM of **C8-SQ/10C8-SQ-DT**, 0.15 mM NB of **PEG$_4$-NB**, 0.15 Mm DT of **PEG$_4$-DT**, 0.05 mg/mL of **Au@PEG-DT** and 0.1 mM LAP), and exposed to a LED for 10 min. Afterwards, the solution (3 µL, 0.5 mM) was applied to a freshly glow-discharged lacey carbon 200 mesh Cu grid and the excess liquid was blotted off for 3 seconds at 100% humidity and

plunge-frozen in liquid ethane using a Vitrobot plunge-freezer (FEI VitrobotTM Mark III, Thermo Fisher Scientific, Waltham, MA, USA). Images were recorded on a BM-Ceta (4k x 4k) at a nominal magnification of 73000x (1.34 Ångstrom per pixel) and defocus of -2.0 to -3.0 µm.

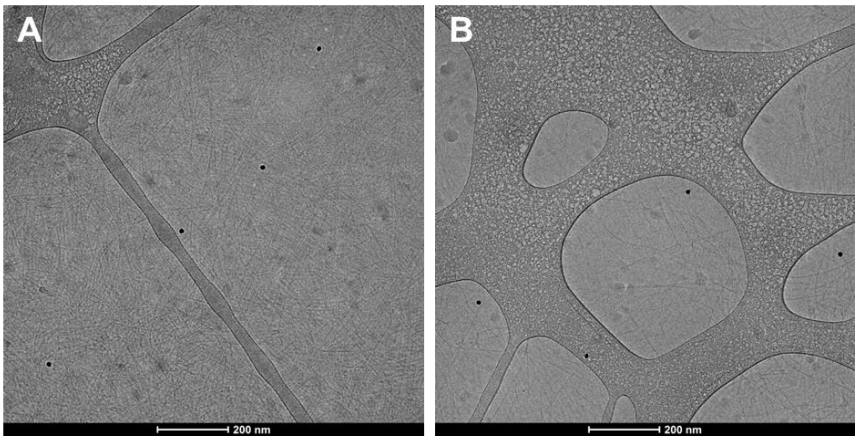

Figure S12. Cryo-TEM images of diluted **DN-Au** hydrogels after UV crosslinking: A) **DN-Au$_{0.25}$** (0.4 mM of **C8-SQ/10C8-SQ-DT**, 0.15 mM NB of **PEG$_4$-NB**, 0.15 Mm DT of **PEG$_4$-DT**, 0.025 mg/mL of **Au@PEG-DT** and 0.1 mM LAP). B) **DN-Au$_{0.5}$** (0.4 mM of **C8-SQ/10C8-SQ-DT**, 0.15 mM NB of **PEG$_4$-NB**, 0.15 Mm DT of **PEG$_4$-DT**, 0.05 mg/mL of **Au@PEG-DT** and 0.1 mM LAP). Scale bar: *200 nm*.

Scanning electron microscope (SEM)

DN and **DN-Au** hydrogels (200 µL) were prepared according to previously established uncross-linked gelation protocol, then exposed to a LED for 10 min. All the samples were lyophilized and fractured in liquid N_2 prior to SEM image. The pore diameters of the hydrogel nanostructures were measured manually in Fiji/ImageJ.

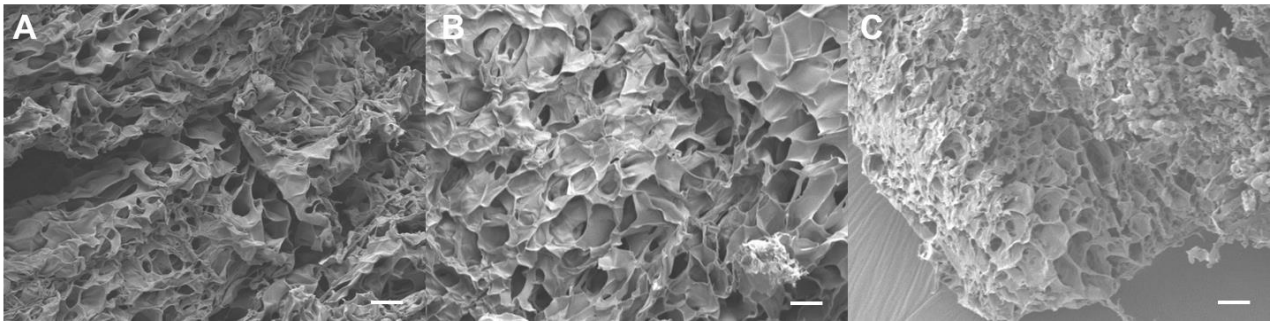

Figure S13. SEM images of **DN** and **DN-Au** hydrogels after crosslinking: (A) **DN**, (B) **DN-Au$_{0.5}$**, (C) **DN-Au$_1$**. Scale bar: *10 µm*.

Equilibrium Swelling ratio and Gel stability test

Hydrogel swelling ratios and gel stability data were acquired by weighing hydrogels at different time points. Hydrogels (100 µL) were prepared according to the gelation protocol in glass vials (2 mL) and crosslinked with a LED for 10 minutes. After crosslinking, the hydrogels were covered with Milli Q water (300 µL) and kept at RT. The weights of hydrogels were recorded at different time points as W*wet*. Hydrogels' W*equ* were recorded when hydrogels were fully swelled to reach swelling equilibrium. After

15 days, the hydrogels were lyophilized and the dried product was weighed as Wdry. Hydrogels swelling ratios was calculated using the formula: $Swelling\ Ratio = (Wequ - Wdry)/Wdry$. Gel stability was calculated using the formula: $Gel\ erosion\% = 100 \times (Wwet - Wdry)/Wequ$. Each test had three parallels.

Conductivity Test

DN and **DN-Au** hydrogels (150 µL) were prepared according to previously established uncross-linked gelation protocol in a non-conductive 9 well Teflon mold with dimensions of 4 mm × 10 mm and at a height of 4 mm, then exposed to a LED for 10 min. Two 2.5 mm x 20 mm Pd electrodes were incorporated into hydrogels at a fixed distance of 8 mm before measurements to provide electrode contact. Here the contacted dimensions of Pd electrodes and hydrogel is 4 x 4 mm. When -Z'' (Ω) reached to 0 Ω, Z'(Ω) was taken to calculate the conductivity by using the formula: $\sigma(S/m) = \frac{0.008}{Z'(\Omega)*2.5*4*0.0001}$.

Photo thermal Test

DN and **DN-Au** hydrogels (150 µL) were prepared according to previously established uncross-linked gelation protocol, then exposed to a LED for 10 min. Milli-Q water (150µL) was placed on top the hydrogels before irradiation with 532 nm laser (1 W) to prevent drying. Temperatures were recorded at different time points to make the curves.

Manual implementation of 3D hydrogel printing

The **DN-Au$_{0.25}$** hydrogel (300 µL) was prepared in a glass vial (2 mL) as described in the gelation protocol without UV irradiation. The uncrosslinked hydrogel was extruded from a micropipetor into water (500 µL) in a glass vial (2 mL). Subsequently, the extruded hydrogel was crosslinked using a LED for 10min. A video was made during the extrusion process and pictures were taken 1 day after crosslinking.

3D cell culture studies

Cell viability tests of NIH 3T3 mouse fibroblasts and bone metastases breast cancer cell-lines (MDA-MB-231-B1). **DN** and **DN-Au** hydrogels were prepared in PBS (pH ~7.4) as described in the gelation protocol without UV irradiation. Cell suspensions were pipetted with hydrogels and seeded in 15-well µ-Slide Angiogenesis plates (Ibidi) at a cell density of 10^6 cells/mL. The hydrogels were crosslinked with UV light by a LED for 5 min, cell medium (50 µL) was then pipetted on top of the hydrogels and was replaced every hour for the first three hours to remove excess LAP. Hereafter, medium was replaced once a day. Before application of the LIVE/DEAD staining, the medium on top of the hydrogels was then removed before washed with 50 µL of PBS for twice. Subsequently, staining solution (40 µL of 2 µM calcein AM and 1.5 µM propidium iodide) was added and incubated for 40 min at 37 °C. The supernatant was replaced with PBS before imaging. Cells were counted using the Fiji/ImageJ macro written for 3D analysis of live and dead cells.

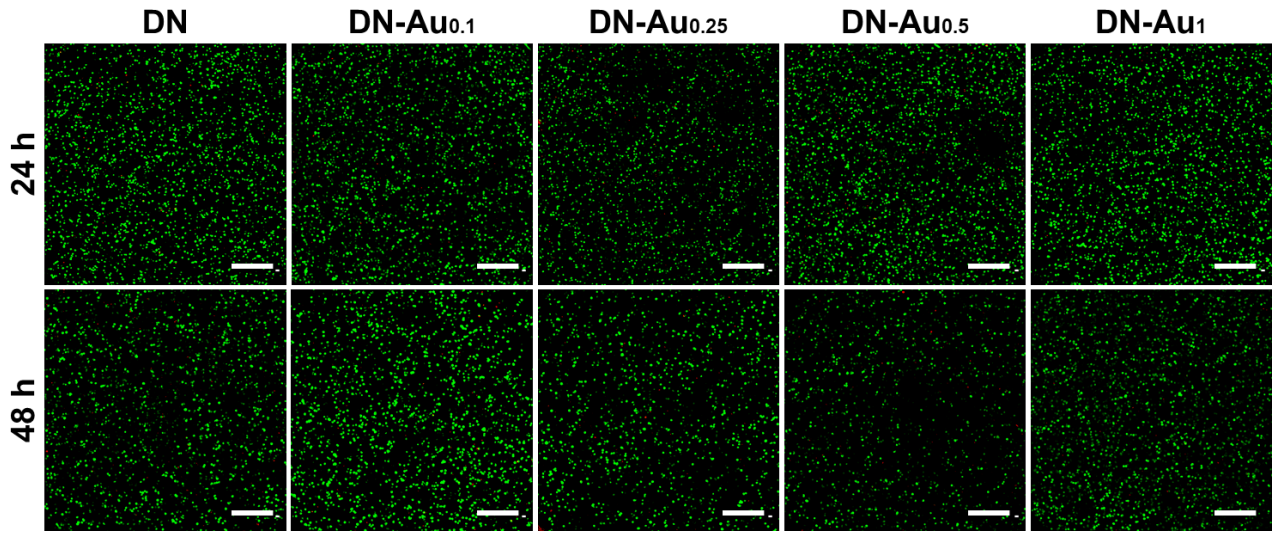

Figure S14. Confocal imaging of NIH 3T3 mouse fibroblasts viability in **DN** and **DN-Au** hydrogels for 24 h and 48 h. Calcein AM (green) and propidium iodide (red) mark the live and dead cells, respectively. Scale bar: *500 μm*.

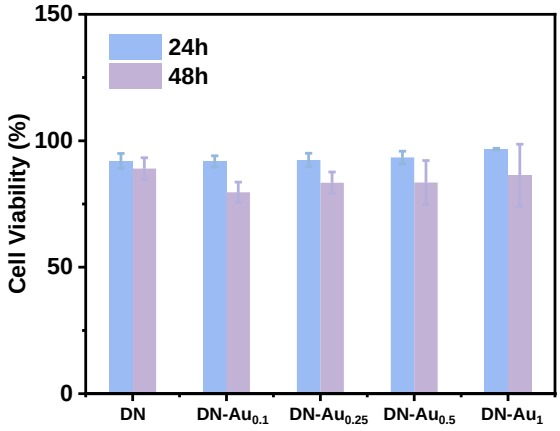

Figure S15. Cell viability of NIH 3T3 mouse fibroblasts encapsulated in **DN** and **DN-Au** hydrogels at 24 h and 48 h. Mean ± SD, N = 3.

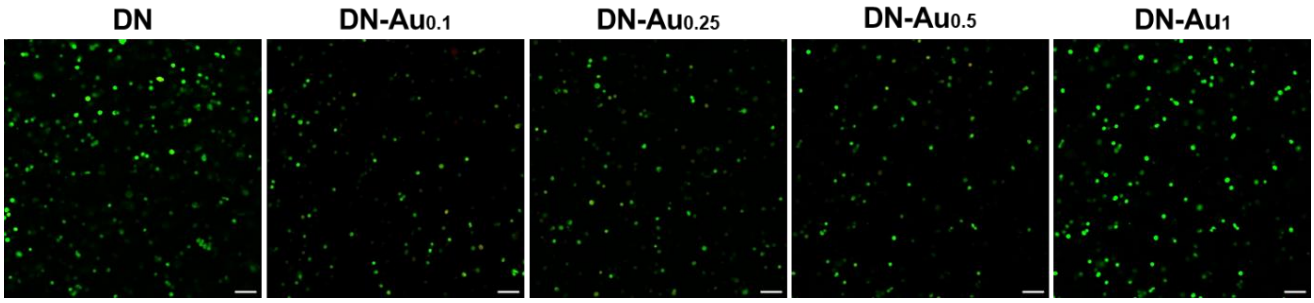

Figure S16. Confocal microscopy images of MDA-MB-231 cells encapsulated in **DN** and **DN-Au** hydrogels for 24 h without different 532 nm laser irradiation. Calcein AM (green) and propidium iodide (red) mark the live and dead cells, respectively. Scale bar: *100 μm*.

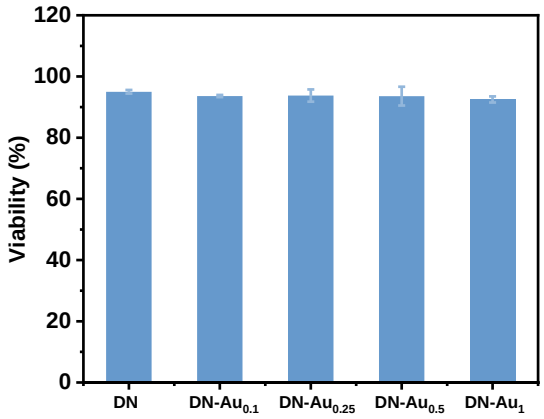

Figure S17. Cell viability of MDA-MB-231-B1 cells encapsulated in **DN** and **DN-Au** hydrogels for 24 h. Mean ± SD, N ≥ 3.

3D phototherapy *in vitro*

Agarose hydrogels (3%, 350 µL) were first prepared in 24-well plates. A hole was made in the center of the agarose hydrogel, with dimensions of 8mm diameter and 1mm height, which was used to seed the cell-laden hydrogels. **DN** and **DN-Au** hydrogels were prepared in PBS (pH ~7.4) as described in the gelation protocol without UV irradiation. Cell suspensions were pipetted with hydrogels and seeded at a cell density of 10^7 cells/mL. The hydrogels were crosslinked with UV light from a benchtop LED (375 nm, ~ 10 mW/cm^2) for 5 min, cell medium (500 µL) was then pipetted on top of the hydrogels and was replaced every hour for the first three hours to remove excess LAP. 24 h later, cell-laden hydrogels were carefully washed with PBS (twice, 500 µL), placed in µ-Slide 8 well plates with PBS (50 µL) inside, and irradiated using a visible light laser at 532 nm with a beam spot of ~6 mm in diameter at a power of 1 W for different time. After the PBS was removed, the staining solution (200 µL of 2 µM calcein AM and 1.5 µM propidium iodide) was immediately added and incubated for 40 min at 37 °C. The supernatant was replaced with PBS before imaging.

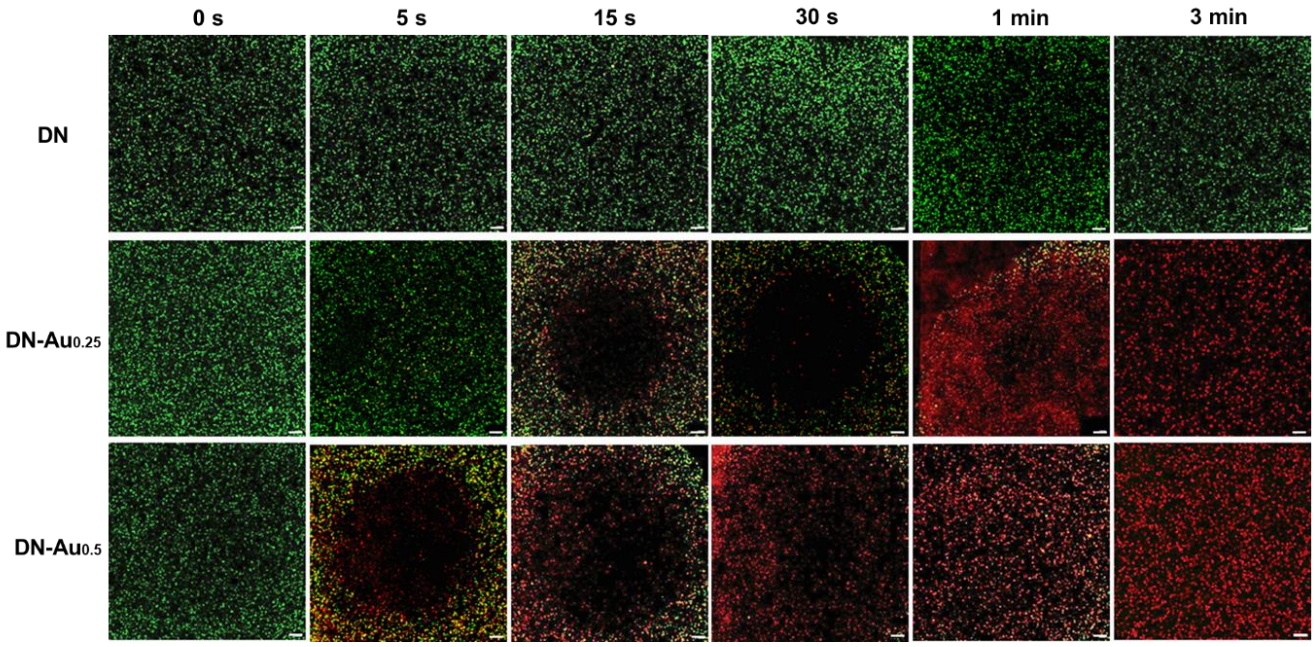

Figure S18. Confocal microscopy images of MDA-MB-231-B1 cells encapsulated in **DN**, **DN-Au$_{0.25}$** and **DN-Au$_{0.5}$** hydrogels after 24 h with different 532 nm laser irradiation. Calcein AM (green) and propidium iodide (red) mark the live and dead cells, respectively. Scale bar: *200 µm*.

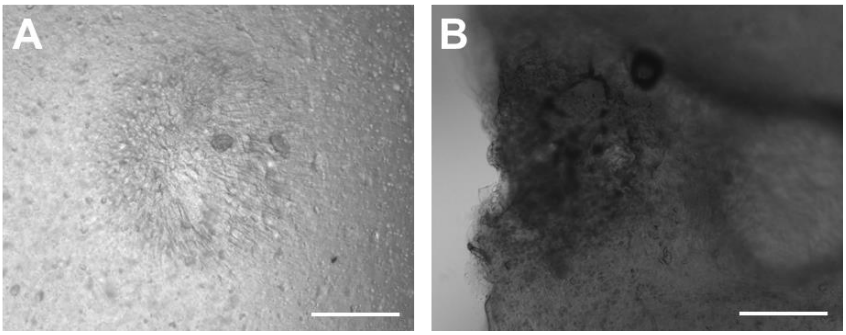

Figure S19. Confocal microscopy images of burned **DN-Au$_{0.25}$** hydrogel encapsulated with MDA-MB-231-B1 after different 532 nm laser irradiation time. (A) 30 s (B) 1 min. Scale bar: *500 µm*.

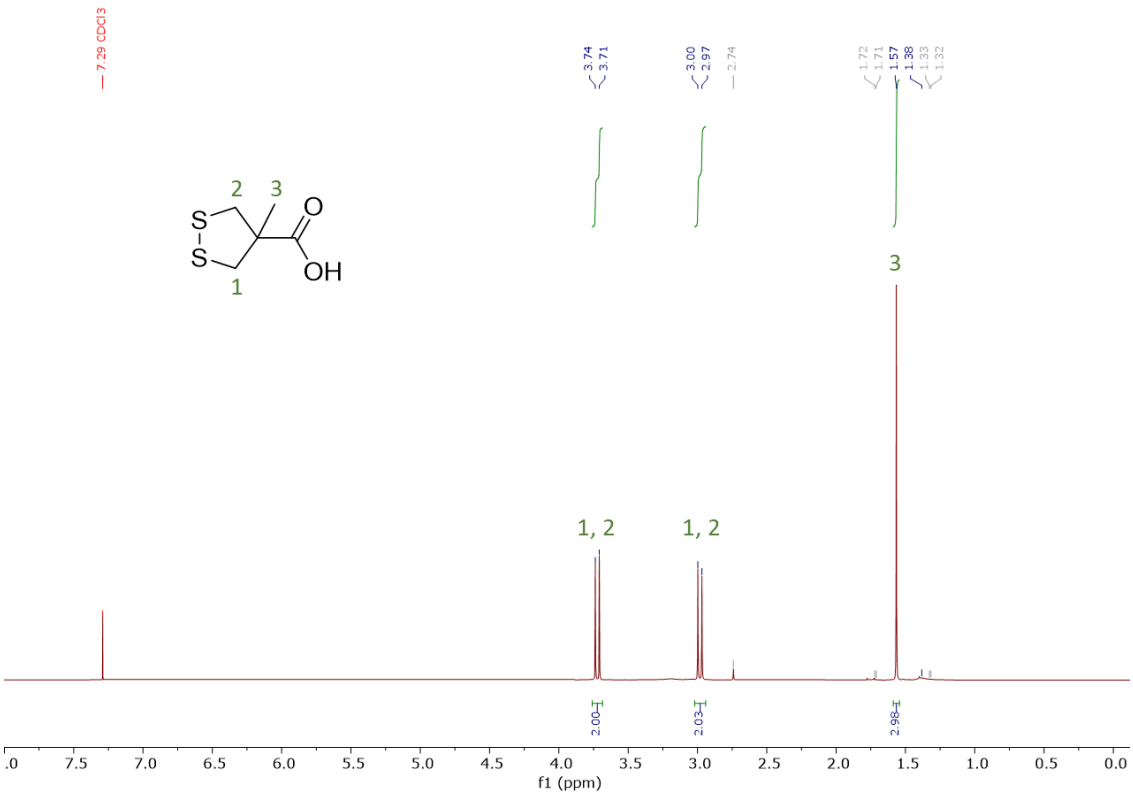

Figure S20. ^{1}H-NMR (400 Hz, 298K, $CDCl_3$) spectrum of **DT**.

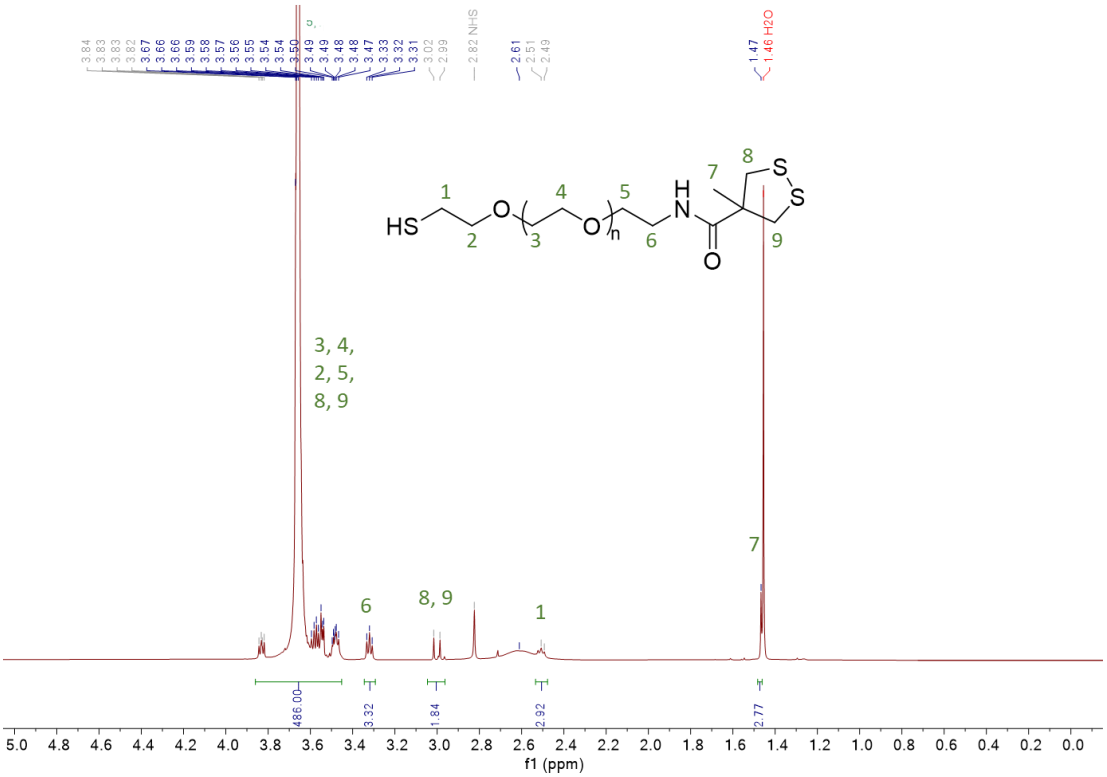

Figure S21. ^{1}H-NMR (400 Hz, 298K, $CDCl_3$) spectrum of **HS-PEG$_{5400}$-DT**. The degree of functionalization was 92%.

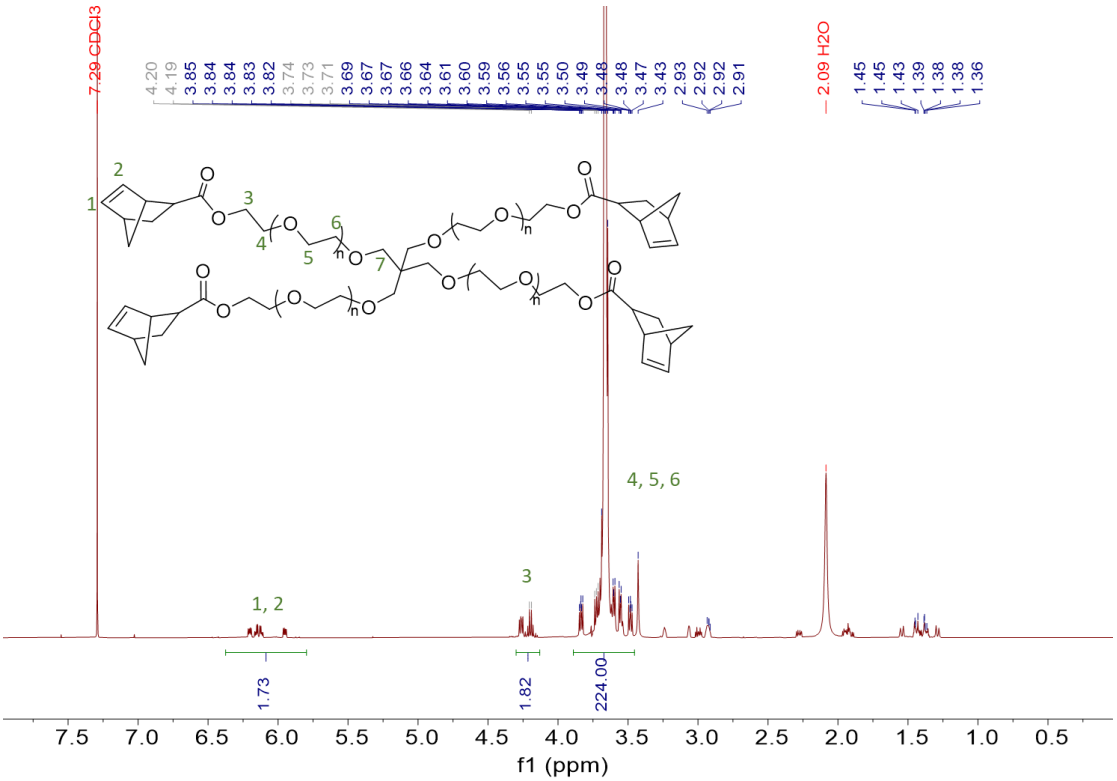

Figure S22. ^{1}H-NMR (400 Hz, 298K, $CDCl_3$) spectrum of **PEG$_4$-NB**. The degree of functionalization was 91%.

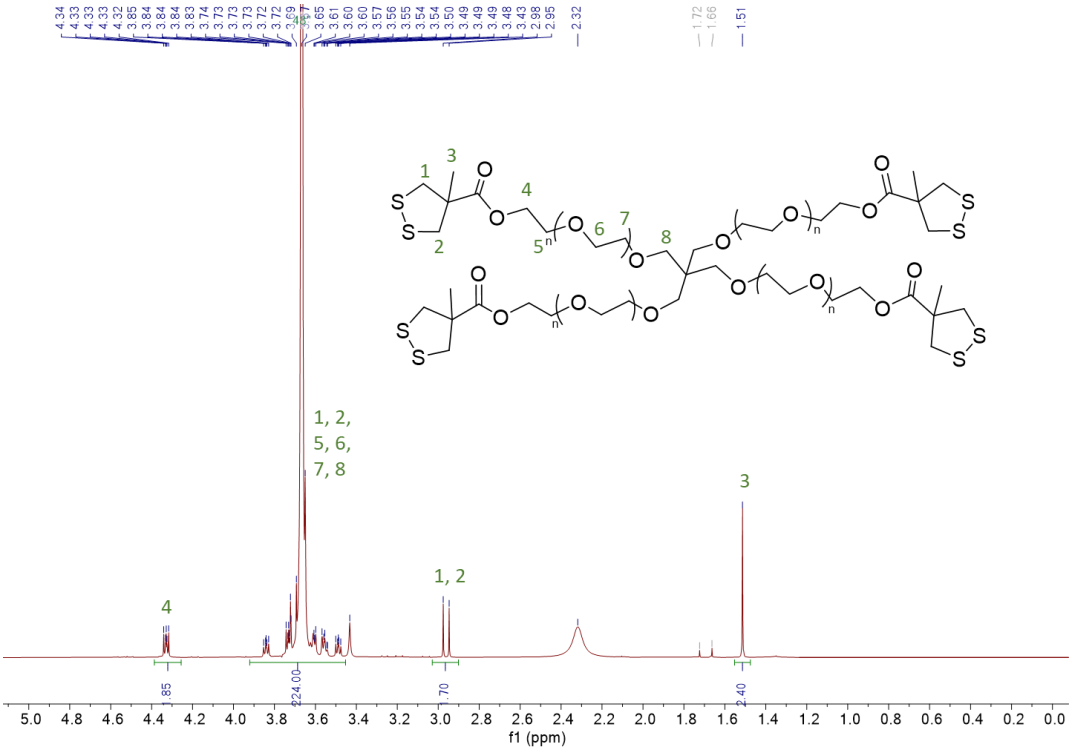

Figure S23. ^{1}H-NMR (400 Hz, 298K, $CDCl_3$) spectrum of **PEG$_4$-DT**. The degree of functionalization was 92%.

Reference

(1) Tong, C.; Wondergem, J. A. J.; van den Brink, M.; Kwakernaak, M. C.; Chen, Y.; Hendrix, M.; Voets, I. K.; Danen, E. H. J.; Le Devedec, S.; Heinrich, D.et al. Spatial and Temporal Modulation of Cell Instructive Cues in a Filamentous Supramolecular Biomaterial. *ACS Appl Mater Interfaces* **2022,** *14* (15), 17042.

(2) Tong, C.; Liu, T.; Saez Talens, V.; Noteborn, W. E. M.; Sharp, T. H.; Hendrix, M.; Voets, I. K.; Mummery, C. L.; Orlova, V. V.; Kieltyka, R. E. Squaramide-Based Supramolecular Materials for Three-Dimensional Cell Culture of Human Induced Pluripotent Stem Cells and Their Derivatives. *Biomacromolecules* **2018,** *19* (4), 1091.

(3) Marat, X. L.-L., K.; Marrot, L. Administration of Dithiolane Compounds for Photoprotecting the Skin. *US8530511B2* **2013**.

(4) JOHN TURKEVICH, P. C. S., JAMES HILLIE. A study of the nucleation and growth processes in the synthesis of colloidal gold. *SYNTHESIS OF COLLOIDAL GOLD* **1951**.

(5) FRENS., G. Controlled Nucleation for the Regulation of the Particle Size in Monodisperse Gold Suspensions. *Nature Physical Science* **1973,** *241(105)*, 20.

(6) Thambiliyagodage, C. Ligand exchange reactions and PEG stabilization of gold nanoparticles. *Current Research in Green and Sustainable Chemistry* **2022,** *5*.